

Development of a Universal Correction Algorithm for Use with any Filter-Based Absorption Photometers (amt-2019-336)

Reply to Anonymous Referee #1:

We appreciate the reviewer's time in reviewing our submission and are grateful for the comments and questions the reviewer provided. These appear to be related to some confusion that the reviewer had in reading our manuscript, which highlights to us that we were not as clear as we should have been with some of the text. We apologize for this lack of clarity and provide clarification in our response to the specific comments below.

- The algorithm is shown in Eq. (9) Looks interesting although quite complicated. How did you get AAE into it? Please show intermediate steps from Eqs. (8) to (9). I read the supplement but did not find steps leading to Eq. (9).

There are no intermediate steps between Equations 8 and 9, and in re-reading our text, we understand why the reviewer has this expectation.

Equation 8 represents a generalized form of both the Bond and Virkkula correction equations, i.e., for either formulation of $f(\text{Tr}(\lambda))$ present in the literature. Equation 9 is our new proposed correction equation for the “g term” in Equation 8, which was developed as a multiple linear regression using $\ln(\text{Tr})$, SSA, and AAE with interaction terms. To clarify, we have modified the text in [Line 345](#) to read “We define a *new* function “g” that can be used in Eq. (8). Specifically, we construct a multivariate linear model for “g”, introducing AAE as a dependent variable and including interaction terms between SSA, AAE, and $\ln(\text{Tr})$...”

- The remainder of the reviewer's comments are related to Bond et al. (1999), which was updated in Ogren (2010), and Virkkula et al. (2005), updated by Virkkula (2010).

First, we would like to clarify that we refer to as “updated B1999” and “updated V2005” are not simply the updated corrections in Ogren (2010) and Virkkula (2010). Those updated corrections are what we refer to as “B1999” and “V2005” in e.g., Figure 2. For our “updated B1999” and “updated V2005” results, we have re-fit the coefficients using the respective “g functions” from those papers, yielding a new set of coefficients that we provided as Table S7. We have added a new section (Section 2.4.3) to indicate that our updates are based on new coefficients rather than the adjustments from Ogren (2010) and Virkkula (2010).

Line 316: “2.4.3 Refitting the coefficients in B1999 and V2005

With the reference measurements of B_{abs} from the photoacoustic instruments, we are able to refit the coefficients in the B1999 and V2005 corrections (C_2 to C_7 in Eq. (5) and Eq. (6)) using our data. Specifically, we use the Levenberg-Marquardt algorithm (1944) to iteratively fit the coefficients until the chi-square of the coefficients are minimized. The fitting is implemented using the “Curvefit” function in Igor Pro. It is worth noting that the derived coefficients may only be valid for the SGP and FIREX data. For aerosol properties different from our study, the optimal coefficients are likely to be different from the ones reported here. Hereafter, the B1999 and V2005

results with refitted coefficients are referred to as “updated B1999” and “updated V2005”, respectively.”

This appears to be the root of the reviewer’s concern, but we provide additional information below.

Response to the reviewer’s first and second observations on Figure 2 and Table 3:

- If I compare the scatter plots in Fig. 2a of V2005 where the B1999 correction was used as such, with Fig. 3 in Virkkula (2010) where the B1999 correction with the coefficients updated by Ogren 2010 the regression lines don't change nearly as much as in your Fig. 2. The difference between the original B1999 and that adjusted by Ogren (2010) is not big, definitely not as much as in your Fig. 2. and in Table 3. For instance, now you claim that the slope for the green changes from 2.5 to 1.01 when using the original B1999 formula and the one adjusted by Ogren (2010). That cannot be true. The additional correction factor Ogren (2010) derived was 0.97 ± 0.01 . Otherwise it is B1999. Also in your Table 3 the change of the slope from 2.83 to 1.03 when using either the original V2005 or the corrected constants in Virkkula (2010) is far from realistic. Both of these can easily be tested by using the constants from those papers. I have added some examples below.

The second observation is that in the above-mentioned scatter plots in V2005 and Virkkula (2010) the absorption coefficients calculated with the B1999 correction without and with the updates are either lower than or close to the absorption standard. The V2005 correction and its adjustment in Virkkula (2010) resulted in increasing the absorption close to the 1:1 line of the respective scatter plots, not decreasing like in your Fig. (2). This is obvious especially for dark aerosol with SSA < 0.3 in those two papers.

Since Ogren (2010) and Virkkula et al. (2010) have respectively adjusted the original corrections (Bond et al. (1999) and Virkkula et al. ((2005))) to universal PSAP spot area and “true” flow rate, we expect the coefficients reported in their publications to be more precise. Thus, we simply use these coefficients when correcting our B_{ATN} data (the coefficients are presented in Table 2), instead of the ones in the original publications. The coefficients provided by the reviewer at the end of the comment are same as the ones reported in Table 2.

Using the coefficients in Table 2 (B1999 and V2005) and Table S7 (B1999 and V2005 updated coefficients), we generated Figure 2 and Table 3. As B_{abs} from the photoacoustic instruments was used as reference when updating the coefficients, the red and blue curves (B1999 and V2005 updated coefficients) are closer to 1:1 in Figure 2 and yield slopes closer to 1 in Table 3.

Reply to the reviewer’s third observation on Figure 2 and Table 3:

- The third observation is that you get essentially the same absorption coefficients with B1999 and V2005 and their respective updates. In Fig 2 the data points are almost on top of each other. And their regression lines are almost identical. This would be correct for high SSA (>0.7) but now your SSA went down to < 0.6 for the FIREX data (your Fig 6) and < 0.5 in the SGP data (your Fig 9). For such low SSA the two methods do not yield so similar absorption coefficients unless you used only data where transmittance > 0.8. What Tr range was used for the regressions?

We definitely agree with the reviewer that the performance of B1999 and V2005 may vary with Tr and SSA. The simulated $B_{\text{abs}}/B_{\text{atn}}$ (“g” term in Eq. 8 and Eq. 9) using different values of Tr and SSA are presented below. The results of B1999 and V2005 are generated using the updated coefficients from Table S7 (FIREX-CLAP). As the reviewer mentioned, the B1999 and V2005 corrections are more agreed for greater values of Tr (as seen in panel d) and the combination of lower values of Tr and greater values of SSA (as seen in panels e and f).

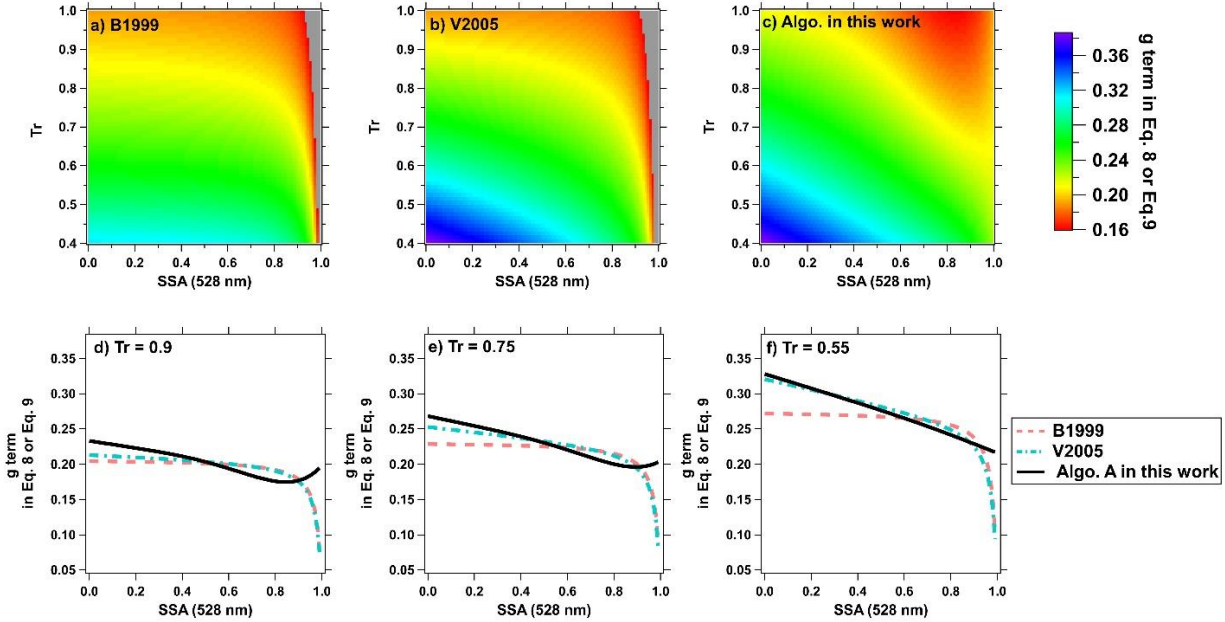


Figure 1. Simulated “g” term (528 nm) in Eq. (8) or Eq. (9). In panel a) and b), the grey regions correspond to “g” values less than 0.16. The results of the B1999 and V2005 are generated using updated coefficients from Table S7 (FIREX-CLAP).

Regarding the reviewer’s comment about the overlap in B1999 and V2005 in Figure 2, we provide the following figures to demonstrate our results. In these figures, B_{abs} derived by the two corrections (467 nm as an example) are plotted against each other, and colored by either SSA (0.3-1) or Tr (0.4-1). Here, we zoom in the original axes (0 - 7000 Mm^{-1}) in Figure 2 to better display our results (0 - 2000 Mm^{-1}). As seen in the figures, the biases between the two corrections are apparently associated with SSA (yet less obvious for Tr), consistent with the trends observed in the previous figure.

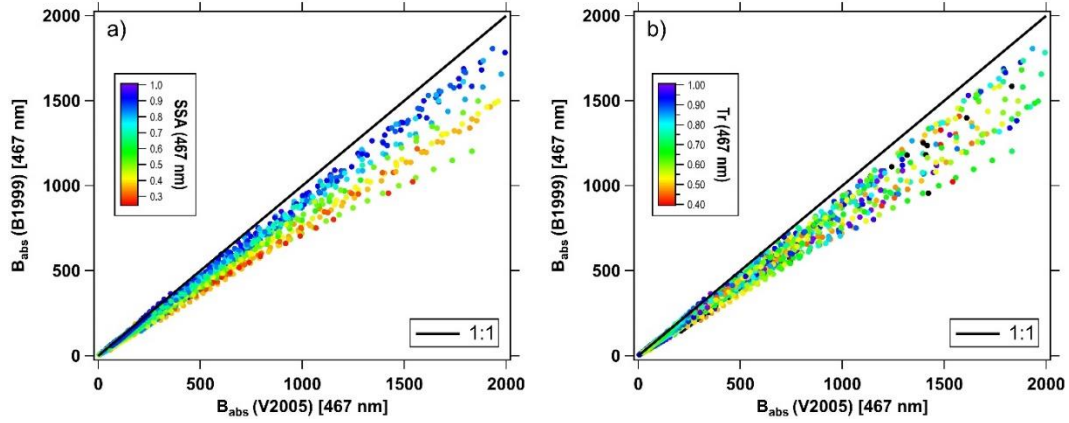


Figure 2. B_{abs} (B1999) against B_{abs} (V2005) for the FIREX data (467 nm). The points are colored by a) SSA and b) Tr. In panel b), there are a few black points, which are associated with $0.25 < \text{Tr} < 0.4$.

We apologize again for some of the ambiguity in our original manuscript regarding B1999, V2005, and our updated versions of both with new coefficients. The revisions prompted by the reviewer's comments have resulted in more clarity within the manuscript, and we thank the reviewer again for his/her comments.

Development of a Universal Correction Algorithm for use with any Filter-Based Absorption Photometers (amt-2019-336)

Reply to Anonymous Referee #2:

We thank the reviewer for the careful reading of our manuscript and for providing a set of very thoughtful comments and critiques, which will be addressed in turn below. Below we restate your editorial comments in italics, and then indicate our response and revision. Please note that all the revised text and references in this response document have been included in the revised manuscript.

The manuscript describes a new correction for filter-based absorption photometers. The method is compared with known correction methods. The authors explain that the method is "universal" due to the wide range of AAEs and SSAs. However, important factors known in the literature are not considered. Details will come later in the review.

Response #1: We first would like to kindly clarify that our intent in calling this a “universal” algorithm is due to its potential application on different filter-based absorption photometers (including PSAP, CLAP, TAP and Aethalometer), rather than its applicability to a wide range of AAE and SSA. The reviewer appears to have captured this intent with her/his final review comment: “*The reviewer has not addressed the application of the new correction to Aethalometers. The reason is that the reviewer is in complete agreement with the authors that there should be a standard method, since the physics in PSAP, CLAP and Aethalometers is the same,*” but this appears to be a different point entirely.

We did try to emphasize our intent for a “universal” algorithm in our original submission, e.g.:

Introduction:

Line 114: In addition, we propose “universal” correction algorithms that are applicable to any filter-based absorption photometer (e.g., CLAP, TAP, PSAP, and AETH) across multiple wavelengths by combining observed filter-based B_{abs} with B_{scat} (e.g., from a co-located nephelometer (NEPH)) and reference B_{abs} (e.g., from a co-located photoacoustic instrument).

Line 136: Our algorithms were then extended to the AETH data from the FIREX laboratory campaign and the PSAP data collected at the SGP site to verify the “universal” nature of the algorithms.

Discussion:

Line 660: Overall, the derived properties using the new correction are consistent across all instruments, suggesting its universality.

Conclusion:

Line 728: We also developed “universal” correction algorithms that are applicable to any filter-based absorption photometer (e.g., PSAP, CLAP, TAP, AETH), which will have utility for any historic or future filter-based absorption measurements and which have the potential to standardize absorption coefficients across all filter-based instruments.

However, this critical disconnect between our intent and the reviewer’s interpretation of our intent exists. To clarify for the reviewer and any other reader of this work, we have added and/or revised text as follows:

We revised the title of our manuscript to “Development of a Universal Correction Algorithm **for Use with any** Filter-Based Absorption Photometer”.

Line 118 (new text): “We emphasize that the “universal” feature of our algorithm is based on its applicability to different filter-based absorption photometers, rather than the ranges of aerosol parameter tested in this work.”

line 337 (new text): “..., but we have the additional aim of developing a model that is applicable to any filter-based absorption photometer.”

Line 562 (revised text, bolded here for emphasis): “**To explore the universal behavior of the new algorithms across different instruments**, we next apply our algorithms to the other filter-based absorption photometers operated during the FIREX study (TAP and AETH).”

The naming of this method in the title as "universal" method is wrong. It remains hidden to the reader that this method has only been developed and tested for specific aerosol types. The limitations are given in the conclusion. Furthermore, it is important to emphasise that the corrected factors for the Bond1999 and Virkkua2005 corrections are only valid for the specific aerosols investigated in this study. An application as a 'standardised' method, as suggested by the authors, is only possible after successful testing with different aerosol types.

Response #2: As we stated above, the so-called “universality” is not based on aerosol properties, so we again apologize for this confusion. Regardless, we do agree with the reviewer that our correction factors derived by B1999 and V2005 are only valid for the aerosols tested in this work. Therefore, we added the following sentence to emphasize this in Line 422: “It is important to keep in mind that the updated coefficient values of B1999 and V2005 (Table S7) are only valid for the aerosols investigated in this study. Future experiments are needed to systematically determine how the coefficients in B1999 and V2005 may change for different aerosol types.”

Moreover, we added a new section (section 2.4.3) describing how we updated the coefficients in B1999 and V2005.

Line 316: “2.4.3 Refitting the coefficients in B1999 and V2005

With the reference measurements of B_{abs} from the photoacoustic instruments, we are able to refit the coefficients in the B1999 and V2005 corrections (C_2 to C_7 in Eq. (5) and Eq. (6)) using our data. Specifically, we use the Levenberg-Marquardt algorithm (1944) to iteratively fit the coefficients until the chi-square of the coefficients are minimized. The fitting is implemented using the “Curvefit” function in Igor Pro. It is worth noting that the derived coefficients may only be valid for the SGP and FIREX data. For aerosol properties different from our study, the optimal coefficients are likely to be different from the ones reported here. Hereafter, the B1999 and V2005

results with refitted coefficients are referred to as “updated B1999” and “updated V2005”, respectively.”

Known correction methods are closely related to physical models. Terms of the corrections are associated with physical effects (e.g. load correction, scattering correction). The model presented here is based more on mathematical optimisation methods. A discussion of the derived parameters (G0 to G7) and how these parameters are related to aerosol properties is missing.

Response #3: We first would also like to correct an error in Eq. 9 which the reviewer highlights by the calculation of $g < 0$ in a later comment: the parameters after G_5 and G_6 ($\ln(\lambda) \times AAE$ and $SSA(\lambda) \times AAE$, respectively) should be exchanged. Eq. 9 should be:

$$g(Tr(\lambda), SSA(\lambda), AAE) = G_0 + G_1 \times \ln(Tr(\lambda)) + G_2 \times SSA(\lambda) + G_3 \times AAE + G_4 \times \ln(Tr(\lambda)) \times SSA(\lambda) + G_5 \times SSA(\lambda) \times AAE + G_6 \times \ln(Tr) \times AAE + G_7 \times SSA(\lambda) \times AAE \times \ln(Tr(\lambda))$$

The coefficient values in Table 4 and in our supplemental computer code were derived using this correct form of the equation, and there was simply an error in this equation in the manuscript text. We apologize to the reviewer for causing this confusion and are very grateful to her/him for bringing this to our attention. (This explains the negative “g values” that the reviewer discusses in a later comment).

Towards this comment, in the original manuscript, the development and interpretation of Eq. 9 were included in the supplementary materials (pages 2-6), as subsections of “model development”. In the main text, we briefly interpreted how these parameters relate to SSA, AAE, and Tr (Line 350). To further relate these parameters with aerosol properties, we add the following sentences:

Line 352: “Although Eq. (9) is developed based on statistical approaches, we attempt to relate this statistical model to physical effects. The coefficients $G_1 - G_3$ are fairly straightforward, as these account for the influence of filter loading (G_1), relative light scattering by the aerosols (G_2), and the brownness of the aerosols (G_3). The interaction terms ($G_4 - G_7$) are more difficult in assigning a physical meaning; however, the interaction between filter loading and relative light scattering (G_4) is might be interpreted as an absolute light scattering by the aerosols on the filter, while the interaction between filter loading and aerosol brownness (G_6) is somewhat analogous to G_4 . The three-way interaction between filter loading, scattering and brownness of aerosols (G_7) is required because of the three two-way interaction terms.

To further this physical interpretation of our statistical model (Eq. 9), we explore the relationship between $\frac{B_{abs}}{B_{ATN}}$ and $\ln(Tr)$, which essentially follows a “ $y = m \cdot x + b$ ” form, where y is $\frac{B_{abs}}{B_{ATN}}$ and x is $\ln(Tr)$. The slope (m) is defined as $G_1 + G_4 \times SSA + G_6 \times AAE + G_7 \times SSA \times AAE$, and the intercept (b) is defined as $G_2 \times SSA + G_3 \times AAE + G_5 \times SSA \times AAE$. Therefore, different combinations of SSA and AAE modulate this relationship between $\frac{B_{abs}}{B_{ATN}}$ and $\ln(Tr)$. For example, loading “black” particles on the filter (e.g., $AAE \sim 1$ and $SSA \sim 0.3$) tends to produce larger values of $\frac{B_{abs}}{B_{ATN}}$, while loading “white” particles on the filter (e.g., $AAE \sim 3$ and $SSA \sim 0.9$) tends to produce smaller values

of $\frac{B_{\text{abs}}}{B_{\text{ATN}}}$ (see Fig. S3 of this work and Fig. 4 in Virkkula et al. (2005)). This relationship becomes more complex when considering, e.g., mixed sulfate and black carbon particles; SSA can be high while AAE is low, and the corresponding $\frac{B_{\text{abs}}}{B_{\text{ATN}}}$ can be variable (also see Fig. S3). Therefore, in order to properly compensate for the effects of loading and aerosol optical properties, a multiple linear regression with interaction terms is introduced in Eq. (9).”

Detailed Review

Line 130: The authors point out the wide range of SSAs and AAEs. However, it is not shown to what extent these variables are correlated in the available data sets. Scatterplots of AAE, SSA and also SAE would provide valuable information. On this basis, an aerosol classification, as shown for example in Schmeisser et al. (2017), could give valuable information to what extent the data set is sufficient for a universal correction.

Response #4: Thank you for this discerning comment. It was our hope that the use of a broader range of SSA and AAE could make this more widely applicable, but as the reviewer has pointed out elsewhere, this will not be strictly true (and we agree!). Regardless, to address this comment, we generated Figure R1 for the SGP data using similar “AAE-SAE space” as that in Cappa et al. (2016) and Schmeisser et al. (2017). In panel a), our data are colored by SSA and the SGP results from Schmeisser et al. (2017) is illustrated by the brown marker and error bars. In panel b), the AAE and SAE results of all NOAA/ESRL sites from Schmeisser et al. (2017) overlap with our SGP data.

Here, we first emphasize that the SGP data used in our work are subsamples of the campaign reported in Schmeisser et al. (2017), but in general, the AAE and SAE values calculated for the SGP site in our work agree well with the values reported for SGP in Schmeisser et al. (2017). Moreover, our results of AAE and SAE overlap with most of the values from the NOAA/ESRL sites, except when marine aerosols or dust contribute to the local aerosol populations. Though none of the NOAA/ESRL sites fall into the clusters of BC or BC/BrC, some of our data can represent the optical properties of aerosols from these clusters. Therefore, we highlight that our algorithm developed by the SGP data *may* have the potential to be generalized to a variety of environmental conditions, but we would need to validate this using observations from more studies. We again emphasize that our intent was to develop an algorithm that is universal across all filter-based absorption photometers, and not universal across all aerosol types, so such a validation is outside the scope of this work.

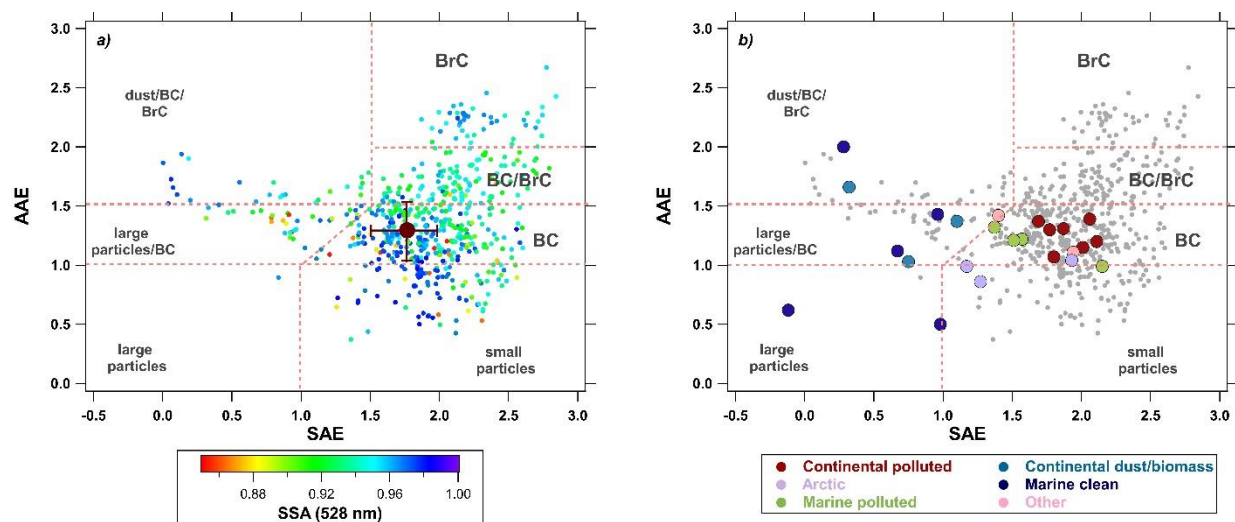


Figure R1. AAE vs. SAE for the SGP data. The three parameters are calculated using photoacoustic B_{abs} and Nephelometer B_{scat} . The panels are overlaid with the classification scheme presented in Cappa et al. (2016) and Schmeisser et al. (2017). In panel a), the averaged values (and standard deviation) of AAE and SAE reported for the SGP site in Schmeisser et al. (2017) are illustrated by the brown marker and error bars. Our results are colored by the corresponding SSA. In panel b), the results in Schmeisser et al. (2017) are colored by the types of observational station and our results are colored in grey.

Figure R1 has been included in the revised supplementary material (Figure S15) and revision was made accordingly:

Line 252: “The scatterplot of AAE and SAE for the SGP data can be found in Fig. S15. Our results of AAE and SAE are compared to the values reported for different NOAA Earth System Research Laboratory (ESRL) observational sites in Schmeisser et al. (2017)”.

Line 608: “To investigate if our algorithms are suitable to correct B_{abs} obtained from different ambient environments, the aerosol properties from the SGP site are compared to those from the other NOAA/ESRL observational sites. We use the similar “AAE-SAE space” as that in Cappa et al. (2016) and Schmeisser et al. (2017) to infer dominant aerosol types (e.g., BC, BrC, dust, mixed dust/BC/BrC, see Fig. S15). ...”

To further investigate how different algorithms apply to different aerosol properties, we generated Figures R2 and R3 (SGP and FIREX, respectively), in which the variable on y axis is B_{abs} ratio = corrected B_{abs} (different corrections) / B_{abs} from photoacoustic instruments (reference), and the parameters on x axis include relative humidity (RH), AAE, SAE, and SSA (528 nm). In general, an apparent association between the B_{abs} ratio and these parameters exists in the uncorrected data (raw B_{ATN}), and this association persists when using B1999 and V2005, especially for RH and SSA. However, these associations are reduced or eliminated when applying our algorithm on the filter-based absorption measurements. Although RH and SAE are not included in our algorithm, our algorithm appears to account for any influence that these parameters have on the measurements. This effect may be captured by one of the interaction terms in our statistical model, but as discussed in Response #3 above, it is difficult to assign physical meaning to these. These figures will also

support our response to some of the reviewer’s comments later in this file (Response #5 and Response #6).

Revision was made accordingly:

Line 375: “We evaluate the model by plotting $\frac{B_{abs}}{B_{ATN}}$ against aerosol properties not included in Eq. (9) (such as relative humidity and aerosol geometric mean diameter, which have been previously reported to bias corrections of filter-based B_{abs} , (Moteki et al., 2010; Nakayama et al., 2010; Schmid et al., 2006)). The results are presented in Fig. S5-S7.”

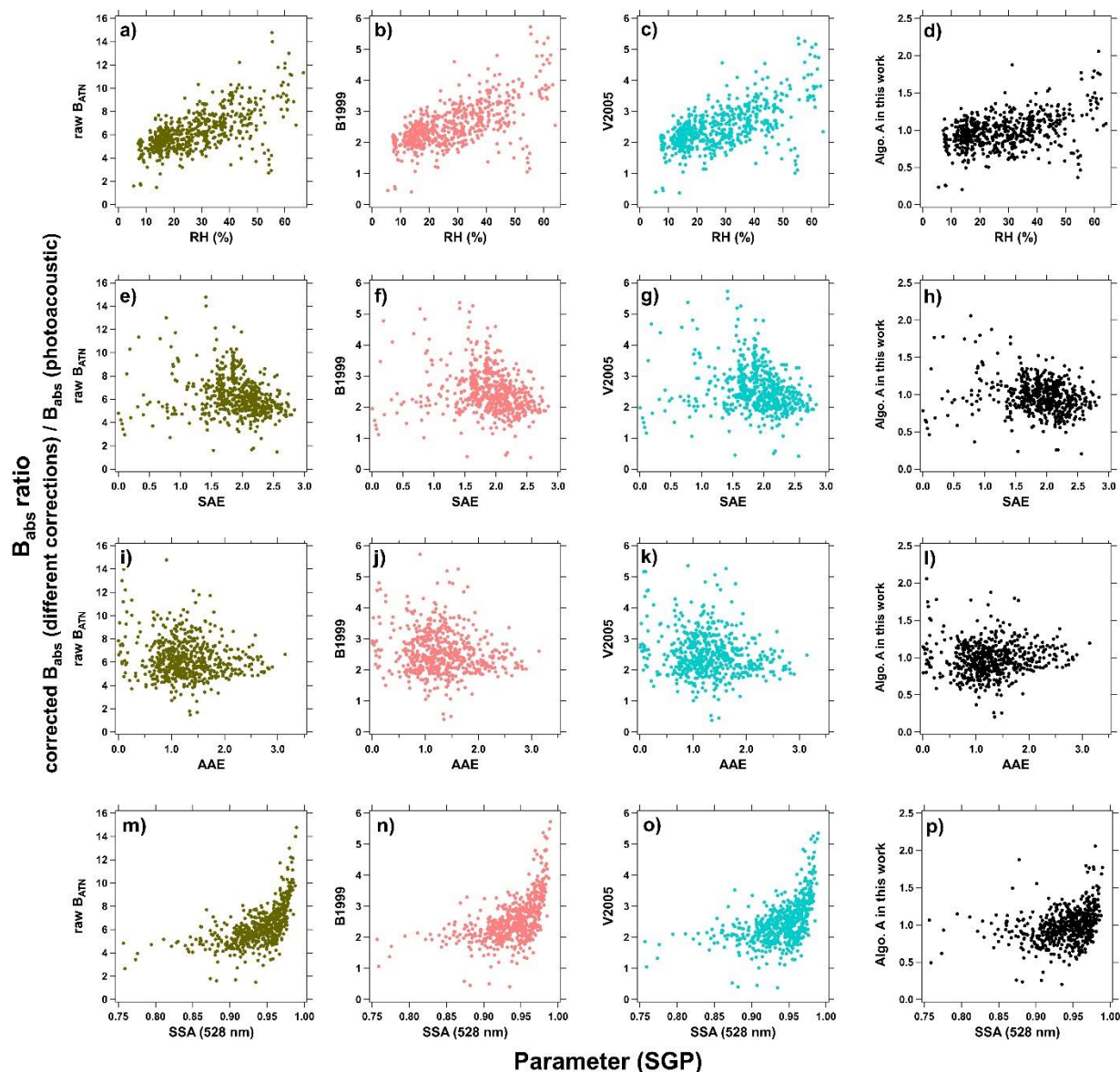


Figure R2. B_{abs} ratio vs. different parameters at the SGP site. In the first column, B_{abs} ratio = uncorrected B_{ATN} / B_{abs} (photoacoustic). In the other columns, B_{abs} ratio = corrected B_{abs} by different corrections / B_{abs} (photoacoustic).

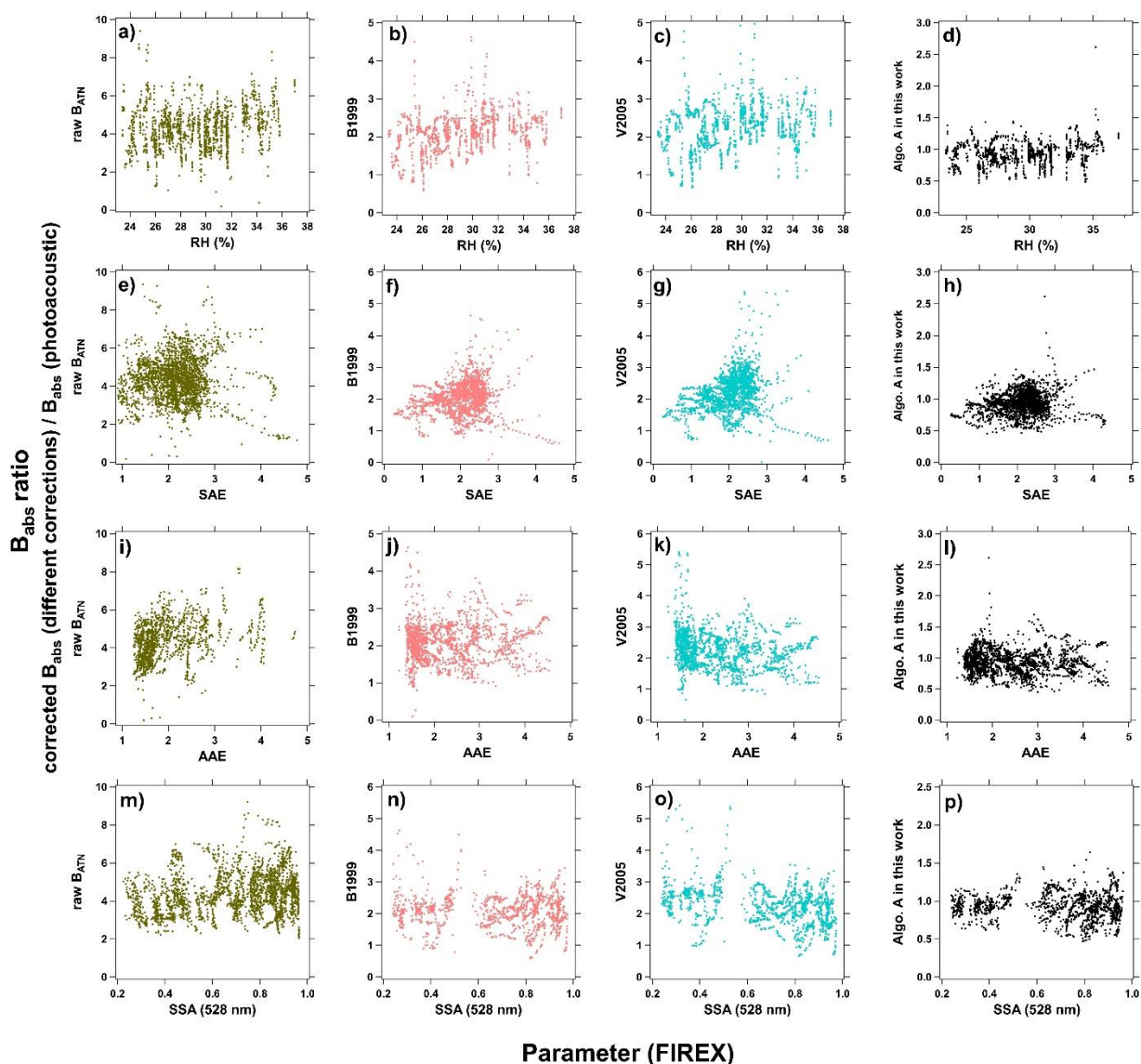


Figure R3. B_{abs} ratio vs. different aerosol properties from the FIREX campaign. In the first column, B_{abs} ratio = uncorrected $B_{\text{ATN}} / B_{\text{abs}}$ (photoacoustic). In the other columns, B_{abs} ratio = corrected B_{abs} from different corrections / B_{abs} (photoacoustic).

Chapter 2: Information on relative humidity or aerosol drying is missing. For developing correction methods, a chapter on instrument calibrations and description of corrections is required.

Response #5: Following the reviewer’s suggestion, we added the information about RH for both datasets (FIREX: 29.3 ± 3.3 , SGP: 26.1 ± 13.9) in a footnote to Table 2. As seen in Figures R2 and R3, our algorithm appears to be able to account for any RH effects. However, we admit that the values of RH for both datasets are relatively low, so extrapolating our algorithms to more humid environments may introduce uncertainties.

Regarding instrument calibration, we agree with the reviewer that it is important when developing correction methods. Thus, when estimating the overall uncertainty of our algorithm in Section 3.5 of the original version, we considered calibration uncertainties (such as the accuracy of the operating wavelengths and the properties of the calibration materials) as part of the measurement uncertainties.

We admit that the instrument calibration procedure was not clearly described in the method section of the original version. It is now revised as following:

Line 230: “Section 2.3. Calibrations

Following Bond et al. (1999) and Ogren et al. (2010), the filter-based instruments were calibrated and corrected for sample area, flow rate, and filter type (see Li et al. (2019) for the FIREX data and Sherman et al. (2015) for the SGP data). Other than that, we did not do any verification beyond the manufacturer's calibration for the filter-based instruments. The SGP nephelometer measurements were corrected for truncation effects (Sherman et al., 2015). The FIREX photoacoustic measurements were calibrated by ammonium sulfate aerosol and fullerene soot (Li et al., 2019).”

A consideration of the particle size effect is missing. It is known that smaller particles can penetrate deeper into the filter and absorb more light there by multiple scattering by the filter material. This effect was theoretically illustrated in Moteki et al (2010) and Nakayama et al (2010) and has been shown in laboratory measurements. According to Nakayama et al., this effect would explain differences of a factor of 2 and greater for mono disperse aerosol. This effect is unfortunately the worst quantified effect for complex aerosols. For the present manuscript this means that without a particle number size distribution of the particles containing absorbing material, the magnitude of the effect cannot be estimated. A correction is only possible with a complex aerosol physical characterization. Nevertheless, possible artefacts due to this effect should always be discussed.

Response #6: We agree with the reviewer that aerosols with different particle sizes may result in different penetrating depth in the filter. For the FIREX data, we had SMPS-derived size distribution (14.6 – 736.5 nm, mobility diameter), so we generated Figure R4 to investigate how number-based geometric mean diameter (d_{pg}) of aerosols affects the corrections' performance. Arguably, the pattern for the B1999 and V2005 data agrees with those reported in Moteki et al. (2010) and Nakayama et al. (2010), in that absorption tends to be over-estimated for smaller particles and that this effect is gradually reduced with increasing particle size. Unfortunately, the size distribution of SGP aerosols is unavailable during our target time period, so we cannot extend this analysis to those data.

Compared to B1999 and V2005, the B_{abs} ratio derived by our new correction is much close to unity when plotting against d_{pg} . Although d_{pg} was not considered when developing the algorithm, any effects related to particle size appear to be captured by our algorithm, potentially in one of the interaction terms (like RH and SAE were above). Unfortunately, we do not have a strong qualitative physical explanation for this.

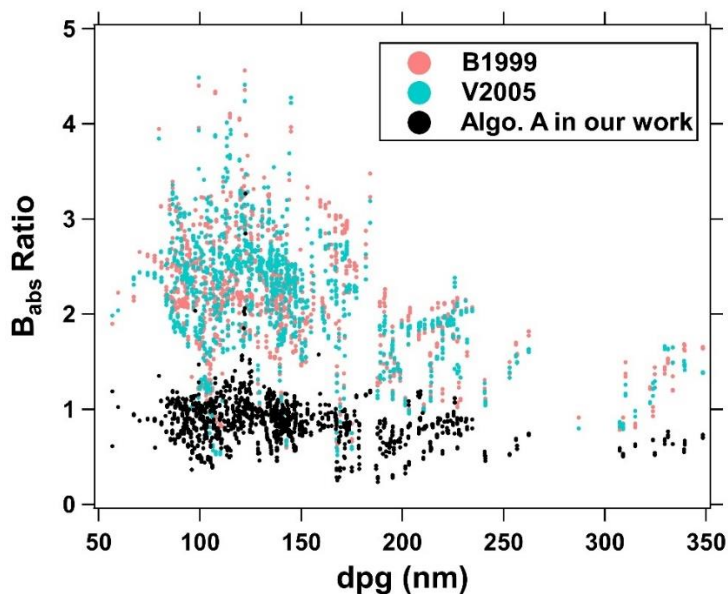


Figure R4. B_{abs} ratio vs. d_g from the FIREX campaign.

*The cross-sensitivity to scattering is important for high SSAs. The Magnitude depends on particle size and wavelength (wavelength effect can be seen in Müller et al., 2011a). It was shown with radiative transfer calculations (Mueller et al., 2014) that this effect is linked to the scattering asymmetry parameter. In Mueller et al. (2014) it was also shown that for high SSAs ($SSA > 0.95$) the corrections become strongly nonlinear and are only insufficiently described by current correction methods. This can also be found in equation 8 of the present manuscript. The second term in 'g' is $(1-ssa)/(1-(1-c1)*ssa)$. In what range of SSAs equation 9 is a good approximation of equation 8?*

Response #7: This is an excellent comment. To compare Eq. 9 to Eq. 8, we produce the Figure R5 to compare the simulated “g” term from our correction and the previous corrections. In panels R5a and R5b, we use the original coefficients reported in B1999 and V2005 to simulate the “g” term in Eq. 8. In panels R5c and R5d, we use the updated B1999 and V2005 coefficients from our Table S7 (FIREX-CLAP). When simulating Eq. 9 (panel R5e), we estimate AAE as a function of SSA ($AAE = a + b \times SSA^c$), similar to the procedure of “Algorithm C” in our manuscript. Then, we plot the results of “g” derived by all corrections as a function of SSA (panels R5f – R5h: $Tr = 0.9, 0.75,$ and 0.5).

In general, the values of “g” term from all corrections increase with decreasing Tr and SSA. However, the figure suggests that there are variations among the corrections for different combinations of Tr and SSA. For example, the original B1999 and V2005 corrections tend to yield greater values of “g” than the other corrections (eventually, insufficient correction), and the agreement between them gets worse as Tr and SSA decrease (panels R5f - R5h). Another observation from the figure is that our correction is in better agreement with the updated B1999 and V2005, but this agreement depends on both SSA and Tr . For example, when $SSA > 0.95$, our correction does not exhibit as strong of a non-linearity as the updated B1999 and V2005. Hence,

Eq. 9 is a good approximation of Eq. 8 when SSA < ~0.95, and the non-linearity is dampened compared to Eq. 8 as SSA approaches unity. We have added this discussion to the updated SI.

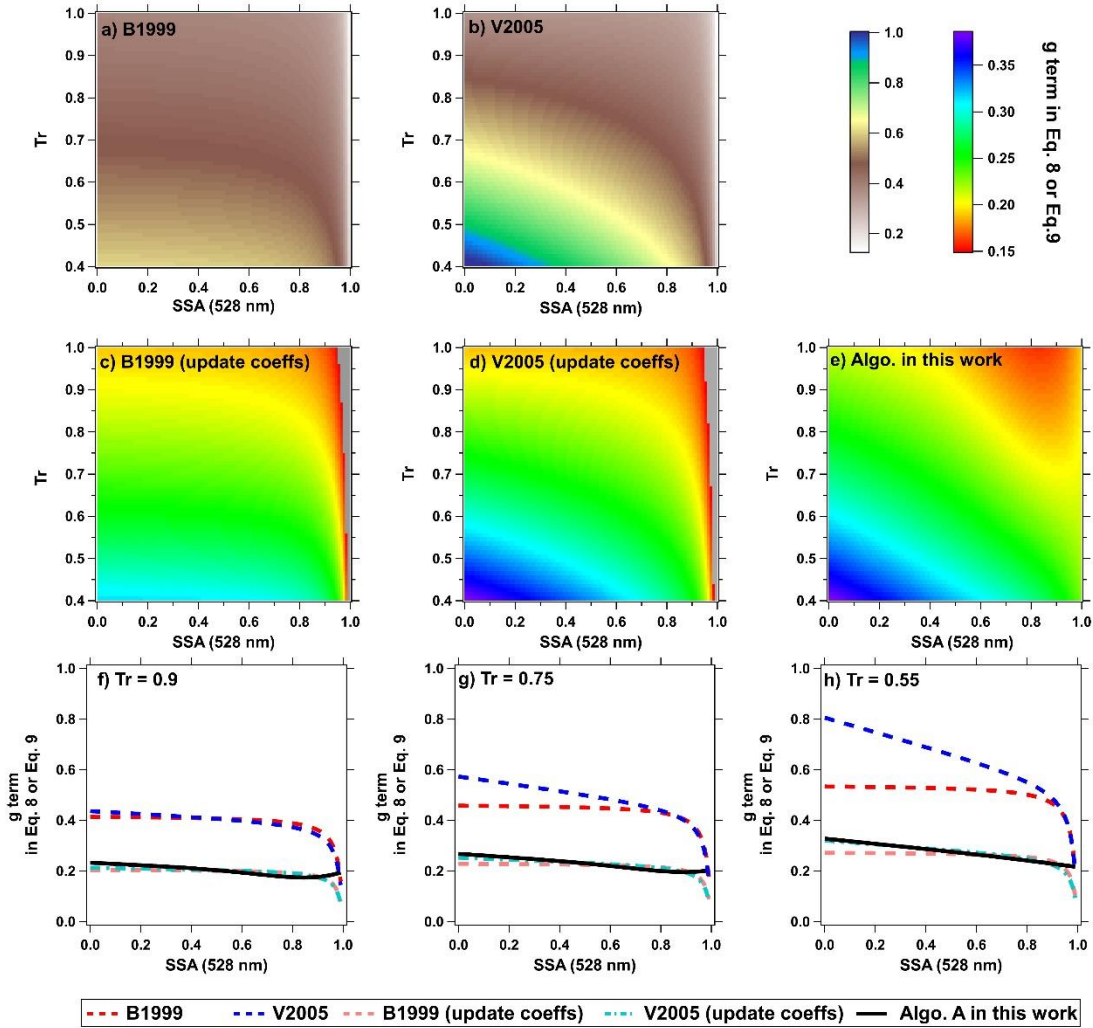


Figure R5. Simulated “g” term in Eq.8 or Eq. 9. In panel c) and d), the grey regions correspond to “g” values less than 0.15.

The approach in equation 9 is a linear equation with interaction terms. According to radiative transfer calculations, this approach makes sense only in a limited range of parameter values. Why AAE is used as independent parameter is not quite obvious. Light scattering and absorption are independent for each wavelength. An indirect dependence on the aerosol type (e.g. composition) is possible. Unfortunately, the parameters and constant are only treated mathematically. A link to aerosol properties would be welcome. This could result in further boundary conditions for the mathematical fit and a more robust determination of the values of the constants might be possible.

Response #8: There are three reasons why we included AAE as an independent variable, which are summarized as follows, in order of importance:

- 1) We found that a model with only SSA and Tr could not well explain the variation of $B_{\text{abs}} / B_{\text{ATN}}$ (discussed briefly in Response #3). As the reviewer indicated, aerosol type may play a role. To incorporate aerosol composition in our correction, we proposed to use AAE because AAE can provide information about aerosol brownness, and it can be inferred from the filter-based instrument (so no additional instruments are needed).
- 2) AAE allows for the implementation “Algorithm C” when there are no measurements of B_{scat} to compute SSA.
- 3) Incorporating AAE into our correction allows to correct B_{abs} at multiple wavelength simultaneously, while the previous corrections treat them separately.

To the reviewer’s point, Figure R2 above does suggest that $B_{\text{abs}} / B_{\text{ATN}}$ is independent of AAE. However, different combinations of SSA and AAE result in different values of this ratio, e.g., as in Figure S3b, reproduced and annotated here:

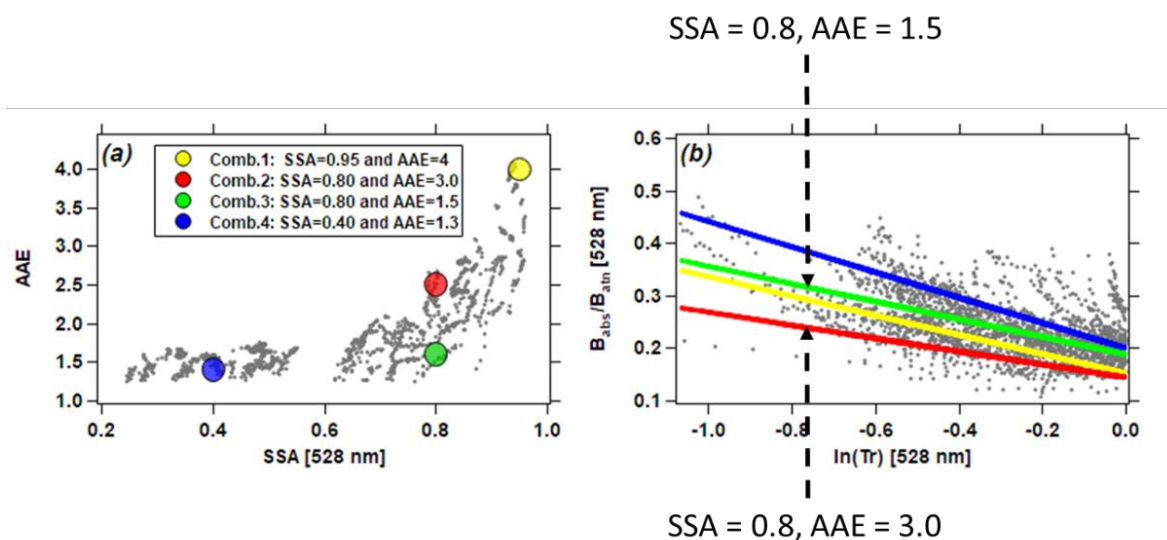


Figure S3. Simple slopes analysis of cross-level interaction of SSA and AAE in predicting $\frac{B_{\text{abs}}}{B_{\text{ATN}}}$ as a function of $\ln(\text{Tr})$ at 528 nm.

Hence, both of these curves differ with a constant offset of ~ 0.1 , with the only difference being the value of AAE used in the computation. We also note that Schmid et al. (2006) and Kim et al. (2019) demonstrate a dependency of AAE on one of the terms used in the Weingartner et al. (2003) correction algorithm for the aethalometer.

In Li et al (2019) the FIREX data set has already been discussed under a different aspect. It was shown that PAX generally provides lower values than other instruments (TAP, CLAP, Offline, EC/OC, SP2). The authors wrote: "This could imply that most instruments over-estimate BC concentrations, but it could also imply that the PAX-870 measurement is incorrect. However, in the absence of a "ground truth" measurement, we cannot confirm or reject either claim. These discrepancies between instrument cannot be explained by measurement uncertainties alone." This gives rise to two possibilities: a) aerosol type or b) larger experimental uncertainties than expected from instrumental uncertainties

a) The special properties of the generated aerosol types are responsible for discrepancies during FIREX. Biomass burning is a challenge. Especially since the different types of instruments measure different properties! The PAX and CLAP/PSAP measure the light absorption and are therefore comparable in principle. It is correct to consider PAX as a reference instrument, because filter based methods require complex corrections. The available data for the FIREX campaign must therefore be considered as being very specific and cannot be used as a universal calibration.

b) The discrepancies between PAX and PSAP/CLAP (see Fig. 5 in Li et al. 2019) for "Black" cluster like particles are significantly higher for the FIREX experiment than values from the literature. These differences require a precise presentation of the calibration, data processing and possible cross-comparisons to underline the high quality of data. Differences due to artefact of measurement techniques should be discussed in detail.

Response #9:

We appreciate the reviewer's comment on this manuscript and our previous work. As stated earlier in this reply, the aerosol properties from the biomass burning are not used to demonstrate the "universal" characteristic. We utilize the FIREX aerosols as they are very important class of absorbing particles that can be examined in the context of the correction. To clarify that the set of coefficients from the FIREX campaign that we are suggesting is appropriate for biomass burning, we add a footnote below Table 4:

Footnote text: "The coefficients derived from FIREX may be more appropriate for biomass burning aerosols, and the coefficients derived by SGP may be more appropriate for rural background environments in the absence of marine aerosols and dust (see Fig. S15)".

To our knowledge, FIREX is the only biomass burning comparison between PAX and PSAP/CLAP that out there (Tasoglou et al. (2018) compared PAX/MAAP). Although the aerosols from the black cluster in Li et al. (2019) tends be more similar to "pure" BC compared to the other two clusters, these aerosols may be still different from the BC used in the previous studies (such as OA/eBC and AAE). Specifically, that comparison in Figure 5 from Li et al. (2019) includes aerosols from flame-generated soot (using, e.g., propane) and internal combustion engines.

Line 198: From which instrument was the scattering Angström exponent (SAE) calculated? Where scattering data corrected for truncation?

Response #10: For the FIREX data, we calculated SAE using B_{scat} measured by the two Photoacoustic Extinctionmeters (PAX): 405 and 870 nm. For the SGP data, we calculated SAE using B_{scat} measured by the Nephelometer (450, 550, and 700 nm).

The Nephelometer- B_{scat} at SGP was corrected for truncation effects (Sherman et al. 2015). During the FIREX campaign, there was a cyclone on the inlet of the sample barrel; thus, the sampled aerosol were generally sub-micron and truncation correction would be quite minor. Otherwise, we have no way to make a quantitative correction for those data.

The results of the multidimensional fit must be checked for physical meaning. Example Table S7, B1999-SGP-CLAP: The parameters C2 and C3 add up to about 5 for all wavelengths. This represents the correction factor for a fresh filter ($Tr=1$) and black aerosol (negligible scattering). The strong wavelength dependence of C2 and C3, however, contradicts the literature. The results in Virkkula et al (2005) (see Figure 2) do not show such a strong wavelength dependence of calibration constants.

Response #11: Ogren (2010) stated that it was unclear how their correction worked for wavelengths other than 574 nm, as they only tested $1-\lambda$ PSAP. Moreover, while we agree that Virkkula et al. (2005) does show a weak wavelength dependence on correction coefficients, other literature does demonstrate this (e.g., (Drinovec et al., 2017; Kim et al., 2019; Schmid et al., 2006)), so a wavelength dependence of these coefficients is not unreasonable.

These differences between models (and spectral dependencies or lack thereof) largely exists because most of these (e.g., B1999, V2005, ours, along with the Weingartner, Schmid, and others that we touch on in our manuscript) are simply not process-based physical models; they are statistical models informed by data. (M2014 appears to be an exception).

Line 306: Aim 1: The range of values of B_{abs} is not important for any correction. Corrections are function of the optical depth of loaded particles (shown in Mueller et al (2014)). Concentration levels is merely important for performing experiments in an acceptable time and proper signal to noise.

Response #12: We thank the reviewer for this comment. Accordingly, we delete “extend the correction a wider range of B_{abs} ” in Line 338.

Figure 3: Is the SSA given for the respective wavelength or for the wavelength of the reference device, the PAX?

Response #13: The SSA represents the respective wavelengths (652, 528, and 467 nm).

The caption is now revised as: Line 478 (revise text, bolded): “The data points are colored by the corresponding SSA **at the given wavelength**”.

Line 670: In Mueller et al. (2011a) no photoacoustic photometer was used. The "reference" instrument was a MAAP. In Arnott et al. (2005) a slope of 1.6 was determined. The measurements were, to the knowledge of the Reviewer, also performed with "SGP-aerosol". Thus, the aerosol could have similar properties to the SGP measurements performed in this study and would not be a true independent measurement (speculation of the reviewer). Davis et al (2019) compared the B1999, V2005 and M2014 (Mueller et al. 2014) methods. Corrected values with the B1999 and V2005 methods were 40 to 50% higher than values of a PAS. The M2014 method could almost halve the deviations, although the M2014 method is identical to the B1999 and V2005 methods for low SSAs. The improvements are therefore clearly due to the improved scattering correction and probably also to the introduction of a mixed term between scattering and absorption. It would be very interesting to see how the performance of the M2014 method would be for the present FIREX measurements.

Response #14: Unfortunately, we do not have backscattering measurements for the FIREX data (because we used PAX for B_{scat} , instead of Nephelometer); therefore, it appears to not be possible to apply M2014 on the FIREX data. However, to address the reviewer's comments, we tested M2014 using our SGP-CLAP data. The parameters used by us (e.g., δ_{af} , δ_{sf} , μ_1 , χ) are the same as those in Müller et al. (2014) and Davies et al. (2019). We first regenerate Fig. 6 and Fig. 7 in Müller et al. (2014) to validate our coding (see Figure R6 below).

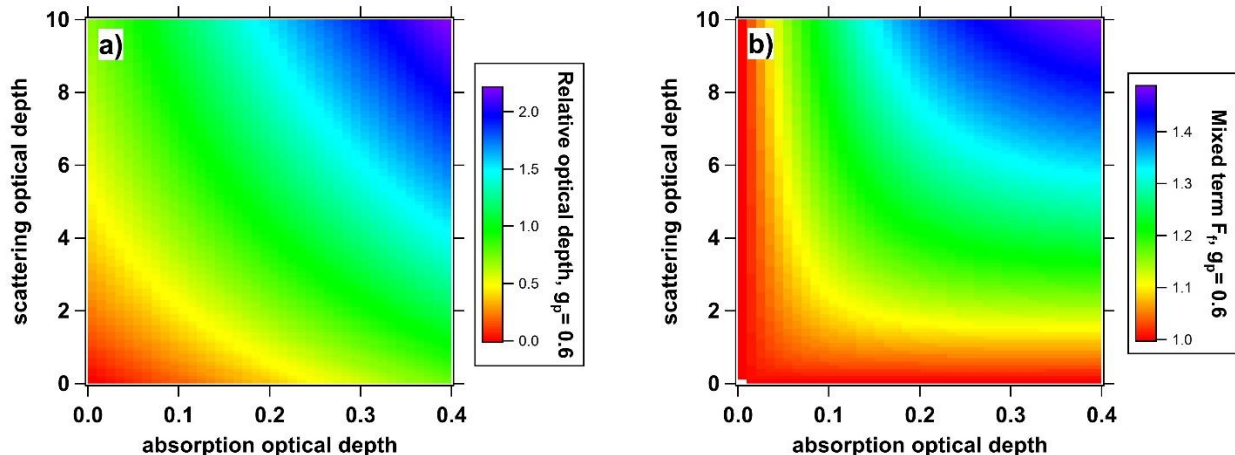


Figure R6. Simulated relative optical depth (panel a) and F_f (panel b) as a function of scattering and absorption optical depths.

As seen in Figure R7, B_{abs} corrected by the M2014 correction agrees fairly well with those derived by the original B1999 and V2005, but overestimates the photoacoustic measurements by factors ~ 2.5 . Another observation is that the performance of M2014 increases as the wavelength decreases that (as seen by the R^2), which is consistent with the results for urban emissions in Davies et al. (2019). We will consider digging deeper to compare the performance of M2014 against the other corrections in the future.

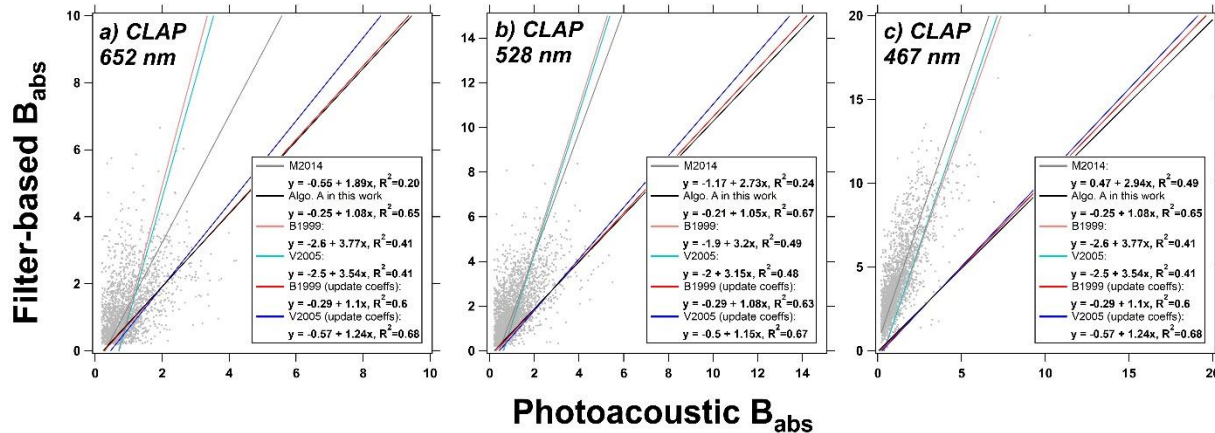


Figure R7. Inter-comparison between the CLAP-derived B_{abs} corrected by the M2014 correction and the reference B_{abs} at 652, 528, and 467 nm for the SGP data. The relationships derived by the other corrections discussed in our manuscript are given in the figure.

Regarding M2014, we make the following revision in our manuscript:

Line 275: “Besides the above mentioned B1999 and V2005 corrections, the constrained two-stream (CTS) correction proposed by Müller et al. (2014) can be also applied on PSAP-similar instruments. The CTS correction was developed based on the relationship between absorption optical depth and B_{abs} . However, it is not straightforward to reformulate the CTS correction as a function of Tr as those presented in Eq. (5) and Eq. (6). Thus, we exclude the B_{abs} results corrected by the CTS correction in the following analysis. For those who are interested in the B_{abs} results corrected by the CTS correction, we provide the correction results of our SGP-CLAP data in Fig. S9.”

Moreover, we agree with the reviewer that the introduction of a mixed term between scattering and absorption may improve the correction performance (**response #8**). This is also our motivation to include the interaction terms in our correction (**response #3**). For example, $SSA \times AAE$ may account for the mixing effects between B_{abs} and B_{scat} .

Line 701: The authors wrote "It is unclear how the algorithms will work for other absorbing aerosols (e.g., dominated by fossil fuel emissions or mineral dust)." There is a simple test. For an unloaded filter ($\ln(TR)=0$) and assuming an aerosol with $SSA=0.9$ and $AAE=1.1$, a not atypical aerosol, g can be calculated using the parameters listed in Table 4. Calculated values are: $g=0.19$ for FIREX/CLAP_green and $g=-0.3$ for SGP/CLAP_green. Negative values are not possible. What has the reviewer done wrong?

Response #15: We thank the reviewer for pointing this out. As mentioned in **response #3**, we realized that there was a mistake in Eq. 9 in the manuscript. Using the revised Eq. 9 and the coefficients in Table 4, we calculate the g term (528 nm) using the values assumed by the reviewer ($\ln(Tr)=0$), $SSA=0.9$, and $AAE=1.1$): FIREX/CLAP: 0.16; FIREX/TAP: 0.47; SGP/CLAP: 0.11; SGP/PSAP: 0.12.

As already indicated, a deeper discussion of the results with regard to aerosol physical properties would be welcome. This could lead to an outlook for further correction models that include the advantages of the individual models.

The reviewer has not addressed the application of the new correction to Aethalometers. The reason is that the reviewer is in complete agreement with the authors that there should be a standard method, since the physics in PSAP, CLAP and Aethalometers is the same.

Response #16: Thank you again for your helpful comments (and we are glad that you are in agreement that there should be some standard method!). We have tried to address the issues raised as best as possible, and we look forward to hearing from you on our manuscript.

References

- Bond, T. C., Anderson, T. L. and Campbell, D.: Calibration and Intercomparison of Filter-Based Measurements of Visible Light Absorption by Aerosols, *Aerosol Sci. Technol.*, 30(6), 582–600, doi:10.1080/027868299304435, 1999.
- Cappa, C. D., Kolesar, K. R., Zhang, X., Atkinson, D. B., Pekour, M. S., Zaveri, R. A., Zelenyuk, A. and Zhang, Q.: Understanding the optical properties of ambient sub- and supermicron particulate matter: results from the CARES 2010 field study in northern California, *Atmos. Chem. Phys.*, 16(10), 6511–6535, doi:10.5194/acp-16-6511-2016, 2016.
- Davies, N. W., Fox, C., Szpek, K., Cotterell, M. I., Taylor, J. W., Allan, J. D., Williams, P. I., Trembath, J., Haywood, J. M. and Langridge, J. M.: Evaluating biases in filter-based aerosol absorption measurements using photoacoustic spectroscopy, *Atmos. Meas. Tech.*, 12(6), 3417–3434, doi:10.5194/amt-12-3417-2019, 2019.
- Drinovec, L., Gregoric, A., Zotter, P., Wolf, R., Anne Bruns, E., Bruns, E. A., Prevot, A. S. H., Favez, O., Sciare, J., Arnold, I. J., Chakrabarty, R. K., Moosmüller, H., Filep, A. and Mocnik, G.: The filter-loading effect by ambient aerosols in filter absorption photometers depends on the coating of the sampled particles, *Atmos. Meas. Tech.*, 10(3), 1043–1059, doi:10.5194/amt-10-1043-2017, 2017.
- Kim, J.-H., Kim, S.-W., Ogren, J. A., Sheridan, P. J., Yoon, S.-C., Sharma, S. and Lin, N.-H.: Multiple scattering correction factor estimation for aethalometer aerosol absorption coefficient measurement, *Aerosol Sci. Technol.*, 53(2), 160–171, doi:10.1080/02786826.2018.1555368, 2019.
- Levenberg, K.: A method for the solution of certain non-linear problems in least squares, *Q. Appl. Math.*, 2(2), 164–168, 1944.
- Li, H., Lamb, K. D., Schwarz, J. P., Selimovic, V., Yokelson, R. J., McMeeking, G. R. and May, A. A.: Inter-comparison of black carbon measurement methods for simulated open biomass burning emissions, *Atmos. Environ.*, 206, 156–169, doi:10.1016/j.atmosenv.2019.03.010, 2019.
- Moteki, N., Kondo, Y. and Nakamura, S.: Method to measure refractive indices of small nonspherical particles: Application to black carbon particles, *J. Aerosol Sci.*, 41(5), 513–521, doi:10.1016/j.jaerosci.2010.02.013, 2010.
- Müller, T., Virkkula, A. and Ogren, J. A.: Constrained two-stream algorithm for calculating aerosol light absorption coefficient from the Particle Soot Absorption Photometer, *Atmos. Meas. Tech.*, 7(12), 4049–4070, doi:10.5194/amt-7-4049-2014, 2014.
- Nakayama, T., Kondo, Y., Moteki, N., Sahu, L. K., Kinase, T., Kita, K. and Matsumi, Y.: Size-dependent correction factors for absorption measurements using filter-based photometers: PSAP and COSMOS, *J. Aerosol Sci.*, 41(4), 333–343, doi:10.1016/j.jaerosci.2010.01.004, 2010.
- Ogren, J. A.: Comment on “Calibration and Intercomparison of Filter-Based Measurements of Visible Light Absorption by Aerosols,” *Aerosol Sci. Technol.*, 44(8), 589–591, doi:10.1080/02786826.2010.482111, 2010.
- Schmeisser, L., Andrews, E., Ogren, J. A., Sheridan, P., Jefferson, A., Sharma, S., Kim, J. E., Sherman, J. P., Sorribas, M., Kalapov, I., Arsov, T., Angelov, C., Mayol-Bracero, O. L., Labuschagne, C., Kim, S.-W., Hoffer, A., Lin, N.-H., Chia, H.-P., Bergin, M., Sun, J., Liu, P. and Wu, H.: Classifying aerosol type using in situ surface spectral aerosol optical properties, *Atmos.*

Chem. Phys., 17(19), 12097–12120, doi:10.5194/acp-17-12097-2017, 2017.

Schmid, O., Artaxo, P., Arnott, W. P., Chand, D., Gatti, L. V., Frank, G. P., Hoffer, A., Schnaiter, M. and Andreae, M. O.: Spectral light absorption by ambient aerosols influenced by biomass burning in the Amazon Basin. I: Comparison and field calibration of absorption measurement techniques, *Atmos. Chem. Phys.*, 6(11), 3443–3462, doi:10.5194/acp-6-3443-2006, 2006.

Sherman, J. P., Sheridan, P. J., Ogren, J. A., Andrews, E., Hageman, D., Schmeisser, L., Jefferson, A. and Sharma, S.: A multi-year study of lower tropospheric aerosol variability and systematic relationships from four North American regions, *Atmos. Chem. Phys.*, 15(21), 12487–12517, doi:10.5194/acp-15-12487-2015, 2015.

Tasoglou, A., Subramanian, R. and Pandis, S. N.: An inter-comparison of black-carbon-related instruments in a laboratory study of biomass burning aerosol, *Aerosol Sci. Technol.*, 52(11), 1320–1331, doi:10.1080/02786826.2018.1515473, 2018.

Virkkula, A., Ahlquist, N. C., Covert, D. S., Arnott, W. P., Sheridan, P. J., Quinn, P. K. and Coffman, D. J.: Modification, calibration and a field test of an instrument for measuring light absorption by particles, *Aerosol Sci. Technol.*, 39(1), 68–83, doi:10.1080/027868290901963, 2005.

Weingartner, E., Saathoff, H., Schnaiter, M., Streit, N., Bitnar, B. and Baltensperger, U.: Absorption of light by soot particles: Determination of the absorption coefficient by means of aethalometers, *J. Aerosol Sci.*, 34(10), 1445–1463, doi:10.1016/S0021-8502(03)00359-8, 2003.

Development of a Universal Correction Algorithm for Use with any Filter-Based Absorption Photometers

Hanyang Li¹, Gavin R. McMeeking², and Andrew A. May¹

¹ The Ohio State University Department of Civil, Environmental, and Geodetic Engineering, Columbus, Ohio, USA

² Handix Scientific, LLC, Boulder, Colorado, USA

Corresponding author: Andrew A. May (may.561@osu.edu).

Abstract

Among the various measurement approaches to quantify light absorption coefficient (B_{abs}), filter-based absorption photometers are dominant in monitoring networks around the globe. Numerous correction algorithms have been introduced to minimize the artifacts due to the presence of the filter in these instruments. However, from our recent studies conducted during the Fire Influence on Regional and Global Environments Experiment (FIREX) laboratory campaign, corrected filter-based B_{abs} remains biased high by roughly a factor of 2.5 when compared to a reference value using a photoacoustic instrument for biomass burning emissions. Similar over-estimations of B_{abs} from filter-based instruments exist when implementing the algorithms on six months of ambient data from the Department of Energy (DOE) Atmospheric Radiation Measurement (ARM) Southern Great Plains (SGP) user facility from 2013 (factor of roughly 3). In both datasets, we observed an apparent dependency on single scattering albedo (SSA) and absorption Ångström exponent (AAE) in the agreement between B_{abs} based on existing correction factors and the reference B_{abs} . Consequently, we developed a new correction approach that is applicable to any filter-based absorption photometer that includes light transmission from the filter-based instrument as well as the derived AAE and SSA. For the FIREX and SGP datasets, our algorithm results in good agreement between all corrected filter-based B_{abs} values from different filter-based instruments and the reference (slopes ≈ 1 and $R^2 \approx 0.98$ for biomass burning aerosols and slopes ≈ 1.05 and $R^2 \approx 0.65$ for ambient aerosols). Moreover, for both the corrected B_{abs} and the derived optical properties (SSA and AAE), our new algorithms work better or at least as well as the two common PSAP-based correction algorithms. The uncertainty of the new correction algorithm is estimated to be $\sim 10\%$, considering the measurement uncertainties of the operated instruments. Therefore, our correction algorithm is universally applicable to any filter-based absorption photometer and has the potential to “standardize” reported results across any filter-based instrument.

1. Introduction

Light-absorbing atmospheric aerosols directly affect the Earth’s energy budget by absorbing solar radiation, leading to a warming effect when they are suspended in the atmosphere and to the melting of snow and ice following deposition (Bond and Bergstrom, 2006; Boucher, 2015; Horvath, 1993). For decades, scientists have conducted field experiments around the globe to investigate how absorbing aerosols influence the atmospheric radiative balance and interact with clouds (e.g., Andrews et al. (2011); Cappa et al. (2016); Lack et al. (2008b); Rajesh and Ramachandran (2018); Schwarz et al. (2008)). These experiments may be performed at fixed stations (e.g., observation sites maintained by the Department of Energy (DOE) Atmospheric Radiation Measurement (ARM)

42 program or the National Oceanic and Atmospheric Administration (NOAA) Global Monitoring
43 Division (GMD)) or on mobile platforms (e.g., car trailer, aircraft, and ship), typically involving
44 the measurements of aerosol chemical, physical, and optical properties. Crucial to the
45 quantification of the radiative forcing of absorbing aerosols are measurements of the absorption
46 coefficient (B_{abs}). For example, long-term monitoring of B_{abs} provides essential data to evaluate
47 chemistry-climate model simulations (e.g., Chen et al. (2019); Vignati et al. (2010)), while
48 intensive measurements of B_{abs} during short-term field campaigns allow for the investigation of
49 optical properties that govern features of aerosol forcing (e.g., McMeeking et al. (2014); Olson et
50 al. (2015)).

51 A variety of instruments have been used to measure B_{abs} , which generally classified into two large
52 categories: filter-based techniques and photoacoustic techniques (Lack et al., 2014; Moosmüller
53 et al., 2009). The major difference between the two categories of technique is that B_{abs} is measured
54 after the aerosols are deposited on the filter media in the filter-based instruments, while the aerosols
55 are characterized within an air stream in the photoacoustic instruments. Compared to the filter-
56 based instruments, the photoacoustic instruments have the advantage of avoiding potential artifacts
57 due to the contact of aerosols with filters; therefore, they are often used as the reference instruments
58 in inter-comparison studies of aerosol absorption (e.g., Arnott et al. (2005); Davies et al. (2019);
59 Jiang et al. (2018); Li et al. (2019); Schmid et al. (2006); Sheridan et al. (2005)).

60 Filter-based absorption photometers have been widely used at observational sites around the world
61 due to their ease of operation and relatively low cost. Numerous instruments can be classified as
62 filter-based absorption photometers including the Radiance Research Particle Soot Absorption
63 Photometer (PSAP), the NOAA Continuous Light Absorption Photometer (CLAP), the Brechtel
64 Manufacturing Tricolor Absorption Photometer (TAP), the Magee Scientific Aethalometer
65 (AETH), and the Thermo Scientific Multi-Angle Absorption Photometer (MAAP). Operationally,
66 all of these instruments are similar in that aerosols are deposited onto a filter and the reduction in
67 the transmission (Tr) of light by the particles (sometimes called attenuation (ATN)) is used to infer
68 B_{abs} . Where the instruments may differ is that some are multi-wavelength (multi- λ) instruments
69 (e.g., 3 λ -PSAP, CLAP, TAP, 7 λ -AETH models), while others are not (e.g., 1 λ -PSAP, other AETH
70 models, MAAP).

71 One challenge with filter-based absorption photometers is that biases can arise due to the presence
72 of the filter. For example, light scattering by particles loaded onto the filter or by the filter itself
73 may affect the transmission of light (e.g., (Arnott et al., 2005; Bond et al., 1999)); non-absorbing
74 material may result in absorption enhancement (e.g., (Cappa et al., 2008)); or organic vapors
75 adsorbed to the filter may itself absorb light (e.g., (Subramanian et al., 2007)). Consequently,
76 various correction algorithms exist to minimize these biases, but they are often specific only to
77 certain instruments. For example, some are applicable to the PSAP, CLAP, and TAP (e.g., (Bond
78 et al., 1999; Müller et al., 2014; Ogren, 2010; Virkkula et al., 2005; Virkkula, 2010)), while others
79 are applicable to the AETH (e.g., (Arnott et al., 2005; Collaud Coen et al., 2010; Drinovec et al.,
80 2017; Kirchstetter and Novakov, 2007; Schmid et al., 2006; Virkkula et al., 2007, 2015;
81 Weingartner et al., 2003)).

82 Although the equations associated with these existing correction algorithms are different, they
83 share some commonalities. For example, the filter-based absorption photometers are assessed
84 using laboratory (e.g., ammonium sulfate, fullerene soot) or ambient aerosols during experiments
85 which include reference measurements of B_{abs} . These reference measurements often include either

86 direct photoacoustic B_{abs} or inferred B_{abs} as the difference between the extinction coefficient (B_{ext})
87 and the scattering coefficient (B_{scat}). Correction equations are developed by comparing data
88 between the filter-based instrument and the reference instrument, where the equations often
89 contain one term that accounts for filter loading effects and another that accounts for multiple-
90 scattering effects. Consequently, the correction equations frequently incorporate both Tr and either
91 B_{scat} or the single-scattering albedo (SSA) to account for these effects. However, even when the
92 correction algorithms are applied, potential issues can remain such as:

- 93 1. Corrected filter-based B_{abs} may remain biased high relative to a reference value of B_{abs} (e.g.,
94 (Arnott et al., 2003; Davies et al., 2019; Lack et al., 2008a; Li et al., 2019; Müller et al., 2011a)).
- 95 2. Comparisons between the reference instrument and B_{abs} corrected by different algorithms can
96 yield variable agreement (e.g., (Collaud Coen et al., 2010; Davies et al., 2019; Saturno et al.,
97 2017)).
- 98 3. Corrected B_{abs} from different filter-based absorption photometers may not agree (e.g., (Davies
99 et al., 2019; Müller et al., 2011a)).
- 100 4. Derived products (such as absorption Ångström exponents (AAE)) may differ based on the
101 implemented correction algorithm (e.g., (Backman et al., 2014; Davies et al., 2019)).
- 102 5. The agreement between measurements of B_{abs} and estimates of B_{abs} by chemistry-climate
103 models may vary based on the implemented correction algorithm (e.g., (Alvarado et al., 2016)).

104 The first three issues in this list may arise due to differences in aerosol optical properties between
105 those used in deriving the correction equation and those associated with a given aerosol sample,
106 and these issues can propagate through to the fourth issue. The final issue is arguably most
107 important because evaluation of chemistry-climate models may be severely affected by the
108 differences between different correction algorithms, which may inhibit the modeling community
109 from providing accurate projections of future temperature and precipitation response.

110 In this work, we seek to address some of these issues. First, we evaluate the CLAP, TAP, and
111 PSAP using two common PSAP-based correction algorithms, namely Bond et al. (1999) as
112 updated by Ogren (2010) and Virkkula et al. (2005) as updated by Virkkula (2010). For brevity,
113 we refer to these corrections as “B1999” and “V2005” for Bond et al. (1999) and Virkkula et al.
114 (2005), respectively, incorporating their respective updates. In addition, we propose “universal”
115 correction algorithms that are applicable to any filter-based absorption photometer (e.g., CLAP,
116 TAP, PSAP, and AETH) across multiple wavelengths by combining observed filter-based B_{abs}
117 with B_{scat} (e.g., from a co-located nephelometer (NEPH)) and reference B_{abs} (e.g., from a co-
118 located photoacoustic instrument). We emphasize that the “universal” feature of our algorithm is
119 based on its applicability to different filter-based absorption photometers, rather than the ranges of
120 aerosol parameter tested in this work. However, in reality (e.g., at long-term observatories),
121 reference values of B_{abs} are rare, and in some cases, complementary B_{scat} measurements may not
122 exist; consequently, we also provide methods to correct filter-based B_{abs} data in these scenarios.
123 To our knowledge, this is the first study to simultaneously evaluate B1999 and V2005 corrections
124 on PSAP “successors” (i.e., CLAP and TAP) and to present a correction algorithm that is broadly
125 applicable to any filter-based absorption photometer. Regarding the latter, even if our correction
126 algorithm has its own limitations, its use can nevertheless standardize the reporting of B_{abs} in long-
127 term datasets.

128 2. Methodology

129 We developed the general form for our correction algorithms using CLAP and TAP measurements
130 collected from biomass burning (65 fires in total) during the Fire Influence on Regional to Global
131 Environments Experiment (FIREX) laboratory campaign in 2016. By using biomass burning
132 emissions, we considered a dataset spanning a broader range of aerosol optical properties (SSA at
133 652 nm: 0.14-0.98; AAE: 1.25-4.73) than has traditionally been used in developing these
134 correction algorithms. We then conducted further evaluation and validation of the model using
135 ambient data, specifically using CLAP measurements from the DOE ARM Southern Great Plains
136 (SGP) user facility in Lamont, OK, USA (02/01/13 to 07/09/13). Our algorithms were then
137 extended to the AETH data from the FIREX laboratory campaign and the PSAP data collected at
138 the SGP site to verify the “universal” nature of the algorithms.

139 2.1. The FIREX campaign

140 2.1.1. Experimental setup

141 In October and November of 2016, we participated in the laboratory portion of the FIREX
142 campaign to investigate the wildfire smoke and their impact on the atmosphere. During the
143 campaign, over 100 burns took place at the U.S. Forest Service’s combustion facility at the Fire
144 Sciences Laboratory (FSL). The fuels burned in this study are representative of western US
145 ecosystems, such as spruce, fir, various pines, and “chaparral” biome (e.g., manzanita, chamise).
146 (See Koss et al. (2018) and Selimovic et al. (2018) for more details).

147 A typical burn lasted for 1-3 hours depending on the smoke sampling strategies (e.g., stack burns
148 versus room burns). During each burn, one or multiple “snapshots” of smoke (typical B_{abs} at 652
149 nm ranged from 100 to 1200 Mm^{-1}) were transferred from the combustion room at FSL into a
150 mixing chamber (210 L) through a long transfer duct (30 m in length, 8” in diameter). The smoke
151 was then diluted by filter air (~230 LPM) in the chamber. Once the concentration in the chamber
152 was stable (detected by the Photoacoustic Extinctionmeter (PAX) which was operated continuously
153 through all fires), the smoke was passed to a suite of instruments to obtain aerosol and gas phase
154 parameters. This chamber also served as an intermediate between the transfer duct and the
155 instrumentation to minimize potential biases that arose due to different sample flow rates and
156 sample locations of the instruments. A more detailed description of our experiments can be found
157 in Li et al. (2019).

158 2.1.2. Measurements of aerosol optical properties

159 During the campaign, five instruments provided measurements of B_{abs} (CLAP, NOAA GMD; TAP,
160 Brechtel Manufacturing Inc. (BMI); Aethalometer (Model AETH-31), Magee Scientific; and two
161 PAXs (Model PAX-870 and PAX-405), Droplet Measurement Technologies) and two instruments
162 provided measurements of B_{scat} (PAX-870 and PAX-405). The instruments included in the present
163 work are summarized in Table 1.

164 Both CLAP and TAP provide B_{abs} measurements of the particles deposited on a filter, similar to
165 PSAP. Different from PSAP, there are multiple filter spots (8 sample spots and 2 reference spots)
166 cycling of one filter in CLAP and TAP, enabling the instruments to run continuously through two
167 or three burns without changing filter. In the CLAP and TAP, sample illumination is provided by
168 LEDs operated at three wavelengths (467, 528, and 652 nm). Here, we apply both B1999 and
169 V2005 to CLAP and TAP data, similar to previous work (e.g., (Backman et al., 2014; Davies et
170 al., 2019)).

171 The key differences between the CLAP and TAP during the FIREX campaign include:

- 172 1. The spot change of the CLAP was manually performed when T_r reached approximately 0.5
173 (or ATN decreased to ~ 69), while the TAP advanced to a new spot automatically with a T_r
174 threshold set to be 0.5.
- 175 2. The spot area, flow rate, and LED-detected wavelengths differed slightly (Table 1).
- 176 3. The CLAP recorded B_{abs} every one minute, while the TAP recorded B_{abs} every ten seconds. To
177 enable the following analysis, we compute the 1-minute averages of TAP-derived parameters.
- 178 4. For the first portion of the campaign (the first 17 days of the 45-day campaign), Pallflex E70-
179 2075S filters were used in the CLAP while Azumi filters (model 371M, Azumi Filter Paper
180 Co., Japan) were used in the second portion of the campaign (due to a lack of availability of
181 the Pallflex filters). The TAP was equipped exclusively with the Azumi filters throughout the
182 campaign. We apply the filter correction recommended in Ogren et al. (2017) to the CLAP and
183 convert from Pallflex to Azumi filters.
- 184 5. BMI substantially re-engineered the CLAP in their development of the TAP.

185 These differences resulted in variable agreement between the CLAP and TAP during FIREX;
186 however, the two instruments did largely agree within experimental uncertainty (e.g., see Fig. S8
187 and Fig. S13 in Li et al. (2019)).

188 A PAX measures B_{abs} and B_{scat} simultaneously for suspended particles using a modulated diode
189 laser. We use these photoacoustic absorption measurements as the reference to evaluate the filter-
190 based B_{abs} and develop our correction algorithms. To enable the evaluation of CLAP and TAP
191 which operate at different wavelengths than the PAXs, we interpolate the measurements of B_{abs}
192 and B_{scat} to the wavelengths of 467, 528, and 652 nm using the values of AAE and scattering
193 Ångström exponents (SAE), similar to Backman et al. (2014) and Virkkula et al. (2005).
194 Theoretically, AAE and SAE fit absorption and scattering as power law functions of wavelength
195 (Bergstrom et al., 2007).

196 Due to the numerous correction algorithms for the Aethalometer (e.g. (Arnott et al., 2005; Collaud
197 Coen et al., 2010; Kirchstetter and Novakov, 2007; Saturno et al., 2017; Schmid et al., 2006;
198 Virkkula et al., 2007; Weingartner et al., 2003)), we do not evaluate these in the present work to
199 limit the scope. In fact, the majority of our focus is the B1999 and V2005 corrections to TAP and
200 CLAP. However, we still test the performance of the new algorithms on the AETH to explore its
201 applicability to that instrument.

202 2.2. Measurements of aerosol optical properties at the SGP observatory

203 The ambient data used in this manuscript are the ground-based aerosol data measured at the SGP
204 observatory from 02/01/13 to 07/09/13 (archived at <https://www.archive.arm.gov/discovery/>). For
205 evaluation purposes, we randomly select a range of dates during which the observations are valid
206 (without incorrect, suspect, and missing data) and the PASS is operated after laser (532 nm)
207 upgrade.

208 At the site, an impactor was used to switch the sampling between two cutoffs (particle diameter
209 $<10 \mu\text{m}$ (PM10) in the first 30 minutes of each hour and $<1 \mu\text{m}$ (PM1) in the latter 30 minutes of
210 each hour). The aerosols exiting from the impactor were dried to RH less than 40% and passed to
211 a CLAP, a PSAP, and two NEPHs. Moreover, a three-wavelength photoacoustic soot spectrometer
212 (PASS-3) was operated at the site and measured B_{abs} and B_{scat} of the aerosols, but these aerosols

213 did not pass through the impactor (e.g., characterizing total suspended particles (TSP)). Typical
214 B_{abs} and B_{scat} reported at the site ranged from 0 to 10 Mm^{-1} and 0 to 50 Mm^{-1} at 550 nm, respectively
215 (e.g., (Sherman et al., 2015)). Although the site is rural (clean background air), long-term transport
216 aerosols (such as mineral dust, absorbing organic aerosols, and secondary organic aerosols (SOA))
217 may affect the local aerosol properties (Andrews et al., 2019).

218 We preprocess the SGP data in three steps. First, due to the systematic difference of aerosol sizes
219 between PASS-derived and filter-based absorption, we only include the PM10 observations,
220 inherently assuming that any differences in the optical properties of PM10 and TSP are negligible.
221 Then, we smooth the 1-second data into 10-minute averages. Thirdly, we estimate the detection
222 limits at each of the three wavelengths in the PASS-3 using the data measured during the
223 “background zero” periods (Allan, 1966) and discard the observations which are below the
224 detection limits. With a 10-min-averaging-time, the detection limits (3σ) for the PASS-3 are 0.78
225 Mm^{-1} (405 nm), 2.01 Mm^{-1} (532 nm), and 0.30 Mm^{-1} (781 nm). For the filter-based instruments,
226 the detection limits are based on previous studies (See Table 1). Moreover, we only retain the
227 observations that satisfy $B_{\text{abs}}(405 \text{ nm}) > B_{\text{abs}}(532 \text{ nm}) > B_{\text{abs}}(781 \text{ nm})$ (or $\text{AAE} > 0$), similar to
228 Fischer and Smith (2018). As with the PAX data from the laboratory, we adjust the PASS-derived
229 B_{abs} to 467, 528, and 652 nm using the inferred AAE values for each 10-minute average.

230 2.3. Calibrations

231 Following Bond et al. (1999) and Ogren et al. (2010), the filter-based instruments were calibrated
232 and corrected for sample area, flow rate, and filter type (see Li et al. (2019) for the FIREX data
233 and Sherman et al. (2015) for the SGP data). Other than that, we did not do any verification beyond
234 the manufacturer's calibration for the filter-based instruments. The SGP nephelometer
235 measurements were corrected for truncation effects (Sherman et al., 2015). The FIREX
236 photoacoustic measurements were calibrated by ammonium sulfate aerosol and fullerene soot (Li
237 et al., 2019).

Table 1 Summary of specifications for instruments relevant to this work.

Instrument	Flow rate (LPM)	Spot area (cm ²)	Type of filter	Measured parameters	Response time	Measurement uncertainty	Detection limit (3 σ , Mm ⁻¹)
PAX-870	1.0	-	-	B _{abs} and B _{scat} (870 nm)	1s	~11% (B _{abs}) ~17% (B _{scat}) (Nakayama et al., 2015)	0.47 (B _{abs}) 0.66 (B _{scat}) ^a
PAX-405	1.0	-	-	B _{abs} and B _{scat} (405 nm)	1s	4% (B _{abs}) 7% (B _{scat}) (Nakayama et al., 2015)	0.27 (B _{abs}) 0.60 (B _{scat}) ^a
PASS-3 ^b	1.0	-	-	B _{abs} and B _{scat} (405, 532, and 781 nm)	1s	4 %, 8 %, and 11 % (B _{abs}) (Nakayama et al., 2015)	0.78 (405 nm) 2.01 (532 nm) 0.30 (781 nm) ^a
NEPH ^b	7.5	-	-	B _{scat} (450, 550, and 700 nm)	1s	10% (Anderson et al., 1996)	0.29 (450 nm) 0.11 (550 nm) 0.17 (700 nm) (5-min average) (Müller et al., 2011b)
CLAP	0.83 ± 0.02 (FIREX) 0.945 (SGP)	0.199 (FIREX) 0.195 (SGP)	Pallflex E70-2075S and Azumi filter (model 371M) ^c	B _{ATN} and Tr ^d (467, 529, and 653 nm)	60s	30% (Ogren et al., 2017)	0.6 (1-min average), 0.12 (10-min average) (Ogren et al., 2017)
TAP	1.26 ± 0.01	0.253	Azumi filter (model 371M) ^c	B _{ATN} and Tr ^d (467, 528, and 652 nm)	10s	30% (Laing et al., 2016)	2.67 (467 nm) 4.11 (528 nm) 2.13 (652 nm) (30-s average) (Davies et al., 2019)
AETH	2.4	0.5	quartz fiber sampling tape	B _{ATN} and Tr (370, 470, 520, 590, 660, 880, and 950 nm)	120s	10% (Sedlacek, 2016)	0.1 (Sedlacek, 2016)
PSAP	1.0	0.178	Pallflex E70-2075W	B _{ATN} and Tr ^d (470, 522, and 660 nm)	60s	~15% (Bond et al., 1999)	0.3 (Springston, 2016)

239 ^a The detection limits of PAX and PASS-3 are determined by Allan deviation analysis (Allan, 1966) of B_{abs} during “background zero”.

240 ^b During the analysis of the data collected at the SGP, we use B_{abs} derived by the PASS and B_{scat} derived by the NEPH to yield the coefficients in the algorithms.

241 ^c Two types of filters were used during the FIREX campaign (See Sect. 2.1.2).

242 ^d The operating wavelengths of CLAP, TAP, and PSAP are stated slightly different by the instrument manufactures. We simply use 467, 528, and 652 nm throughout
243 this manuscript.

244 **Table 2** Overview of the studies of B1999 and V2005 and the description of our experiments.

Study	Aerosol source	SSA subset	Range of B_{abs} (Mm^{-1})	Filter-based instrument for B_{abs}	Reference instrument for B_{abs} ^a	Instrument for B_{scat} ^a	Coefficient values in the correction algorithm ^{b, c}		
The study in B1999	Lab-generated aerosols, including various mixtures of nigrosin and ammonium sulfate	0.5-1 (550 nm)	0-800 (550 nm)	One- λ PSAP (550 nm)	The difference between extinction (OEC) and scattering coefficient (NEPH) ^d	NEPH (450, 550, and 700 nm)	$C_1 = 0.016 \pm 0.023$ (550 nm) $C_2 = 1.55 \pm 0.25$ (550 nm) $C_3 = 1.02 \pm 0.17$ (550 nm)		
The laboratory study in V2005	Lab-generated aerosols, including various mixtures of kerosene soot, ammonium sulfate, and polystyrene latex	0.2-0.9 (530 nm)	0-800 (530 nm)	One- λ PSAP (550 nm), three- λ PSAP (467, 530, 660 nm)	The average of the PA (532 nm and 1064 nm) and the difference between extinction (OEC) and scattering coefficient (NEPH) ^d	NEPH (450, 550, and 700 nm)	467 nm $C_1 = 0.015$ $C_4 = 0.377 \pm 0.013$ $C_5 = -0.640 \pm 0.007$	530 nm $C_1 = 0.017$ $C_4 = 0.358 \pm 0.011$ $C_5 = -0.640 \pm 0.007$	660 nm $C_1 = 0.022$ $C_4 = 0.352 \pm 0.013$ $C_5 = -0.674 \pm 0.006$
The ambient study in V2005	Ambient aerosols measured during RAOS and NEAQS ^e	0.75-1 (530 nm)	0-15 (530 nm)	One- λ PSAP (550 nm), three- λ PSAP (467, 530, 660 nm)	PA (532 nm and 1064 nm)	NEPH (450, 550, and 700 nm)	$C_6 = 1.16 \pm 0.05$ $C_7 = -0.63 \pm 0.09$	$C_6 = 1.17 \pm 0.03$ $C_7 = -0.71 \pm 0.05$	$C_6 = 1.14 \pm 0.11$ $C_7 = -0.72 \pm 0.16$
FIREX ^f	Biomass burning aerosols under relatively controlled laboratory conditions	0.2 -1 (550 nm)	38-1800 (550 nm)	CLAP (467, 529, 652 nm), TAP (467, 528, 653 nm), AETH (370, 470, 520, 590, 660, 880, 950 nm)	PAX (405 nm and 870 nm)	PAX (405 nm and 870 nm)	See Table 4 and Tables S6-S10		
SGP (02/01/13 to 07/09/13) ^{f, g}	Ambient aerosols collected at the SGP user facility in Lamont, OK	0.75-1 (530 nm)	0-8 (550 nm)	CLAP (461, 522, 653 nm), PSAP (470, 522, 660 nm)	PASS (405, 532, and 781 nm)	NEPH (450, 550, and 700 nm)			

245 ^a The operating wavelengths are based on the manufacturer specifications.
 246 ^b The coefficients provided in Table 2 are the values presented in Ogren (2010) and Virkkula (2010), which are updated from Bond et al. (1999) and Virkkula et al. (2005),
 247 respectively.
 248 ^c We reformulate the correction equations in the original publications to agree with Eq. (4)–(6) in this manuscript. C_1 to C_7 are the coefficients in the present work.
 249 ^d OEC is optical extinction cell and PA is the instrument using photoacoustic technique.
 250 ^e RAOS and NEAQS are Reno Aerosol Optics Study and New England Air Quality Study, respectively.
 251 ^f The relative humidity (%) of the sampled aerosols from the FIREX and SGP study is 29.3 ± 3.3 and 26.1 ± 13.94 , respectively.
 252 ^g The scatterplot of AAE and SAE for the SGP data can be found in Fig. S15. Our results of AAE and SAE are compared to the values reported for different NOAA Earth
 253 System Research Laboratory (ESRL) observational sites in Schmeisser et al. (2017).

254 2.34. The correction algorithms
 255 In filter-based instruments, the light intensities transmitted through the sample spot and blank spot
 256 of the filter are recorded as I_s and I_b , respectively. The logarithmic ratio of the two intensities at
 257 time t is defined as ATN using the Beer-Lambert law:

$$258 \quad \mathbf{ATN}(t) = -100 \times \ln \frac{I_s(t)}{I_b(t)} \quad 1$$

259 where $\mathbf{ATN} = 0$ when beginning a new filter spot ($t = 0$).

260 The ATN can be related to \mathbf{Tr} by normalizing I_s/I_b at time t relative to I_s/I_b at the start of a new
 261 filter spot ($t = 0$):

$$262 \quad \mathbf{Tr}(t) = \frac{I_s(t)/I_b(t)}{I_s(0)/I_b(0)} = \exp\left(\frac{-\mathbf{ATN}(t)}{100}\right) \quad 2$$

263 The change of ATN over a time interval (Δt) for the instrument operated at a volume flow rate of
 264 Q and spot area of A yields the attenuation coefficient ($\mathbf{B}_{\mathbf{ATN}}$) for that time interval:

$$265 \quad \mathbf{B}_{\mathbf{ATN}} = \frac{A}{Q \times \Delta t} \times \Delta \mathbf{ATN} \quad 3$$

266 $\mathbf{B}_{\mathbf{ATN}}$ is finally converted to $\mathbf{B}_{\mathbf{abs}}$ by applying correction algorithms. The general form of the
 267 correction algorithms presented for the PSAP in Bond et al. (1999) and Virkkula et al. (2005) can
 268 be summarized as:

$$269 \quad \mathbf{B}_{\mathbf{abs}} = \mathbf{B}_{\mathbf{ATN}} \times f(\mathbf{Tr}) - C_1 \times \mathbf{B}_{\mathbf{scat}} \quad 4$$

270 where $f(\mathbf{Tr})$ is some function of \mathbf{Tr} (that may vary between approaches), correcting for the filter
 271 loading effect. C_1 is a constant that may vary with wavelength; specifically, it is a penalty for the
 272 light scattering by the particles collected on the filter which may contribute to the quantification
 273 of ATN. In most atmospheric and laboratory studies, $\mathbf{B}_{\mathbf{scat}}$ is measured independently, typically
 274 using a co-located NEPH.

275 Besides the above mentioned B1999 and V2005 corrections, the constrained two-stream (CTS)
 276 correction proposed by Müller et al. (2014) can be also applied on PSAP-similar instruments. The
 277 CTS correction was developed based on the relationship between absorption optical depth and $\mathbf{B}_{\mathbf{abs}}$.
 278 However, it is not straightforward to reformulate the CTS correction as a function of \mathbf{Tr} as those
 279 presented in Eq. (5) and Eq. (6). Thus, we exclude the $\mathbf{B}_{\mathbf{abs}}$ results corrected by the CTS correction
 280 in the following analysis. For those who are interested in the $\mathbf{B}_{\mathbf{abs}}$ results corrected by the CTS
 281 correction, we provide the correction results of our SGP-CLAP data in Fig. S9.

282 2.34.1. The B1999 correction

283 Bond et al. (1999) was the first study to present the correction algorithm for filter-based
 284 instruments. This empirical correction was originally developed for the PSAP operated at 550 nm
 285 using various mixtures of laboratory-generated nigrosin ($\text{SSA} \approx 0.5$) and ammonium sulfate (SSA
 286 ≈ 1) with $\mathbf{B}_{\mathbf{abs}}$ ranged from 0 to 800 Mm^{-1} .

287 After calibrating the flow rate and spot area of the PSAP, the authors derived $C_1 = 0.016$ and

$$288 \quad f(\mathbf{Tr})_{\mathbf{B1999}} = \frac{1}{C_2 \times \mathbf{Tr} + C_3} \quad 5$$

289 where $C_2 = 1.32$ and $C_3 = 0.87$ (after combining Eq. (3) and Eq. (12) from Bond (1999)).

290 The equation parameters were further clarified in Ogren (2010) who adjusted the B1999-measured
291 spot area ($A = 20.43 \text{ mm}^2$) to be consistent with the universal area of the PSAP ($A = 17.83 \text{ mm}^2$).
292 Ogren (2010) also extended the correction to 574 nm using a wavelength dependence of B_{abs} (B_{abs}
293 $\sim \lambda^{-0.5}$). Consequently, C_2 and C_3 in $f(\text{Tr})$ were updated to 1.55 and 1.02, respectively. These are
294 the values used in the present work (Table 2) for B1999. Moreover, Ogren (2010) stated that the
295 correction forms of Eq. (4) and Eq. (5) were valid for any wavelength, while additional
296 experiments were needed to establish the equation parameters for the wavelengths other than 574
297 nm.

298 2.3.4.2. The V2005 correction

299 Virkkula et al. (2005) developed a correction algorithm for both three-wavelength PSAP (467, 530,
300 and 660 nm) and one-wavelength PSAP (574 nm) using the same functional form as Eq. (4). Since
301 the operating wavelengths of the photoacoustic instruments and the NEPH were different from
302 those of the PSAP, the measured photoacoustic B_{abs} and B_{scat} was extrapolated or interpolated to
303 467, 530, and 660 nm, using inferred AAE and SAE respectively. In this study, the authors used
304 various mixtures of kerosene soot, ammonium sulfate, and polystyrene latex (SSA ranged from
305 0.2 to 0.9) with B_{abs} ranging from 0 to 800 Mm^{-1} at 530 nm.

306 Different from the $f(\text{Tr})$ in the B1999 correction which was a reciprocal function of Tr , the $f(\text{Tr})$
307 presented in V2005 was a multivariate linear function of the natural logarithm of Tr and SSA
308 (including an interaction term between the two):

$$309 \quad f(\text{Tr}(\lambda), \text{SSA}(\lambda))_{\text{V2005}} = C_4 + C_5 \times (C_6 + C_7 \times \text{SSA}(\lambda)) \times \ln(\text{Tr}(\lambda)) \quad 6$$

310 where the parameters in Eq. (6) vary with wavelengths. The parameters in V2005 were updated in
311 Virkkula (2010) by correcting for flowmeter calibration (Table 2).

312 Due to the unknown values of SSA before deriving B_{abs} , Virkkula et al. (2005) provided a solution
313 through an iterative procedure. In the iteration, B_{abs} is first calculated using the B1999 correction
314 (e.g., Eq. (4) and Eq. (5)) and is then used to compute the initial guess of SSA for use in Eq. (6).
315 The B_{abs} and SSA can be updated using Eq. (4) and Eq. (6) until convergence is reached.

316 2.4.3. Refitting the coefficients in B1999 and V2005

317 With the reference measurements of B_{abs} from the photoacoustic instruments, we are able to refit
318 the coefficients in the B1999 and V2005 corrections (C_2 to C_7 in Eq. (5) and Eq. (6)) using our
319 data. Specifically, we use the Levenberg-Marquardt algorithm (1944) to iteratively fit the
320 coefficients until the chi-square of the coefficients are minimized. The fitting is implemented using
321 the “Curvefit” function in Igor Pro. It is worth noting that the derived coefficients may only be
322 valid for the SGP and FIREX data. For aerosol properties different from our study, the optimal
323 coefficients are likely to be different from the ones reported here. Hereafter, the B1999 and V2005
324 results with refitted coefficients are referred to as “updated B1999” and “updated V2005”,
325 respectively.

326 2.4.4. The new correction

327 We develop a set of new correction algorithms with the same general form as Eq. (4) using the
328 biomass burning emissions from 65 different burns during the FIREX laboratory study, providing

329 a broader range of aerosol optical properties and aerosol concentrations than previous work. This
 330 was motivated by the disagreement that remained between filter-based and photoacoustic
 331 instruments, even after applying B1999 to the data (e.g., see Li et al. (2019) Fig. 4 and our Fig. 2
 332 below). These differences may persist because we were effectively extrapolating the B1999
 333 correction equation to values outside the range for which it was developed.

334 This new correction is developed based on multiple linear regression techniques with three
 335 dependent variables of $\ln(\text{Tr})$, SSA, and AAE and one independent variable of $B_{\text{abs}}/B_{\text{ATN}}$ (Eq. (7)
 336 – (9)). As with other correction equations, this model takes into account the influence of scattering
 337 and weakly-absorbing materials, but we have the additional aim of developing a model that is
 338 applicable to any filter-based absorption photometer. However, we target two additional aims: 1)
 339 extend the correction a wider range of B_{abs} ; and 2) develop a model that is applicable to any filter-
 340 based instrument.

341 Similar to the B1999 and V2005 corrections, this new model starts with the general form of Eq.
 342 (4), re-written here to define B_{scat} in terms of SSA and B_{abs} .

$$343 \quad B_{\text{abs}}(\lambda) = B_{\text{ATN}}(\lambda) \times f(\text{Tr}(\lambda)) - C_1 \times \frac{\text{SSA}(\lambda)}{1 - \text{SSA}(\lambda)} \times B_{\text{abs}}(\lambda) \quad 7$$

344 Re-arranging this equation to move all B_{abs} terms to the left-hand side yields:

$$345 \quad B_{\text{abs}}(\lambda) = B_{\text{atn}}(\lambda) \times g(\text{Tr}(\lambda), \text{SSA}(\lambda)) \quad 8$$

$$346 \quad \text{where } g(\text{Tr}(\lambda), \text{SSA}(\lambda)) = f(\text{Tr}(\lambda)) \times \frac{1 - \text{SSA}(\lambda)}{1 - (1 - C_1) \times \text{SSA}(\lambda)}.$$

347 We define a new function “g” that can be used in Eq. (8). We define the function “g” as a
 348 multivariate linear model. Specifically, we construct a multivariate linear model for “g”,
 349 introducing AAE as a dependent variable and including interaction terms between SSA, AAE, and
 350 $\ln(\text{Tr})$:

$$351 \quad g(\text{Tr}(\lambda), \text{SSA}(\lambda), \text{AAE}) = G_0 + G_1 \times \ln(\text{Tr}(\lambda)) + G_2 \times \text{SSA}(\lambda) + G_3 \times \text{AAE} + G_4 \times \ln(\text{Tr}(\lambda)) \times \text{SSA}(\lambda) +$$

$$352 \quad G_5 \times \text{SSA}(\lambda) \times \ln(\text{Tr}) \times \text{AAE} + G_6 \times \ln(\text{Tr}) \times \text{SSA}(\lambda) \times \text{AAE} + G_7 \times \text{SSA}(\lambda) \times \text{AAE} \times \ln(\text{Tr}(\lambda)) \quad 9$$

353 Equation (9) suggests that different combinations of SSA, AAE and $\ln(\text{Tr})$ can result in the same
 354 value of “g” (i.e., $B_{\text{abs}}/B_{\text{ATN}}$); likewise, a given value of $B_{\text{abs}}/B_{\text{ATN}}$ may have infinitely many points
 355 with distinct slopes passing through it (Fig. S3). Although Eq. (9) is developed based on statistical
 356 approaches, we attempt to relate this statistical model to physical effects. The coefficients $G_1 - G_3$
 357 are fairly straightforward, as these account for the influence of filter loading (G_1), relative light
 358 scattering by the aerosols (G_2), and the brownness of the aerosols (G_3). The interaction terms (G_4
 359 – G_7) are more difficult in assigning a physical meaning; however, the interaction between filter
 360 loading and relative light scattering (G_4) is might be interpreted as an absolute light scattering by
 361 the aerosols on the filter, while the interaction between filter loading and aerosol brownness (G_6)
 362 is somewhat analogous to G_4 . The three-way interaction between filter loading, scattering and
 363 brownness of aerosols (G_7) is required because of the three two-way interaction terms.

364 To further this physical interpretation of our statistical model (Eq. 9), we explore the relationship
 365 between $\frac{B_{\text{abs}}}{B_{\text{ATN}}}$ and $\ln(\text{Tr})$, which essentially follows a “ $y = m \cdot x + b$ ” form, where y is $\frac{B_{\text{abs}}}{B_{\text{ATN}}}$ and x is
 366 $\ln(\text{Tr})$. The slope (m) is defined as $G_1 + G_4 \times \text{SSA} + G_6 \times \text{AAE} + G_7 \times \text{SSA} \times \text{AAE}$, and the intercept

367 (b) is defined as $G_2 \times SSA + G_3 \times AAE + G_5 \times SSA \times AAE$. Therefore, different combinations of SSA
 368 and AAE modulate this relationship between $\frac{B_{abs}}{B_{ATN}}$ and $\ln(\text{Tr})$. For example, loading “black”
 369 particles on the filter (e.g., AAE ~ 1 and SSA ~ 0.3) tends to produce larger values of $\frac{B_{abs}}{B_{ATN}}$, while
 370 loading “white” particles on the filter (e.g., AAE ~ 3 and SSA ~ 0.9) tends to produce smaller values
 371 of $\frac{B_{abs}}{B_{ATN}}$ (see Fig. S3 of this work and Fig. 4 in Virkkula et al.(2005)). This relationship becomes
 372 more complex when considering, e.g., mixed sulfate and black carbon particles; SSA can be high
 373 while AAE is low, and the corresponding $\frac{B_{abs}}{B_{ATN}}$ can be variable (also see Fig. S3). Therefore, in
 374 order to properly compensate for the effects of loading and aerosol optical properties, a multiple
 375 linear regression with interaction terms is introduced in Eq. (9).

376 ~~Therefore, in order to properly compensate for the effects of loading and aerosol optical~~
 377 ~~properties, a multiple linear regression with interaction terms is required.~~ A detailed description of
 378 the procedure for the model development (e.g., variable transformation (from Tr to $\ln(\text{Tr})$),
 379 variable selection using best-subsets and stepwise approaches, and model assessment) is provided
 380 in the Supplementary Material. We evaluate the model by plotting $\frac{B_{abs}}{B_{ATN}}$ against aerosol properties
 381 not included in Eq. (9) (such as relative humidity and aerosol geometric mean diameter, which
 382 have been previously reported to bias corrections of filter-based B_{abs} , (Moteki et al., 2010;
 383 Nakayama et al., 2010; Schmid et al., 2006)). The results are presented in Fig. S5-S7.

384 As in V2005, iteration is required in our algorithm because B_{abs} is dependent on knowledge of
 385 SSA and AAE, which themselves are dependent on B_{abs} . We propose the following iterative
 386 process to update SSA and AAE in the model.

- 387 1. Initialize AAE from B_{ATN} across the three wavelengths ($B_{ATN} \sim \lambda^{-AAE}$) and initialize SSA for
 388 each wavelength using B_{ATN} from the filter-based absorption photometer and B_{scat} from a co-
 389 located NEPH, i.e., $SSA(\lambda) = \frac{B_{scat}(\lambda)}{B_{scat}(\lambda) + B_{ATN}(\lambda)}$.
- 390 2. Yield an initial set of coefficients G_0 through G_7 for each wavelength to calculate $g(\text{Tr}, SSA,$
 391 $AAE)$ in Eq. (9), using one of the Algorithms described in Sect. 2.45.
- 392 3. Calculate B_{abs} for each wavelength using Eq. (8).
- 393 4. Update AAE and SSA using B_{abs} calculated in Step 3.
- 394 5. Derive a new set of coefficient values.
- 395 6. Iterate Steps 3-5 until converged.

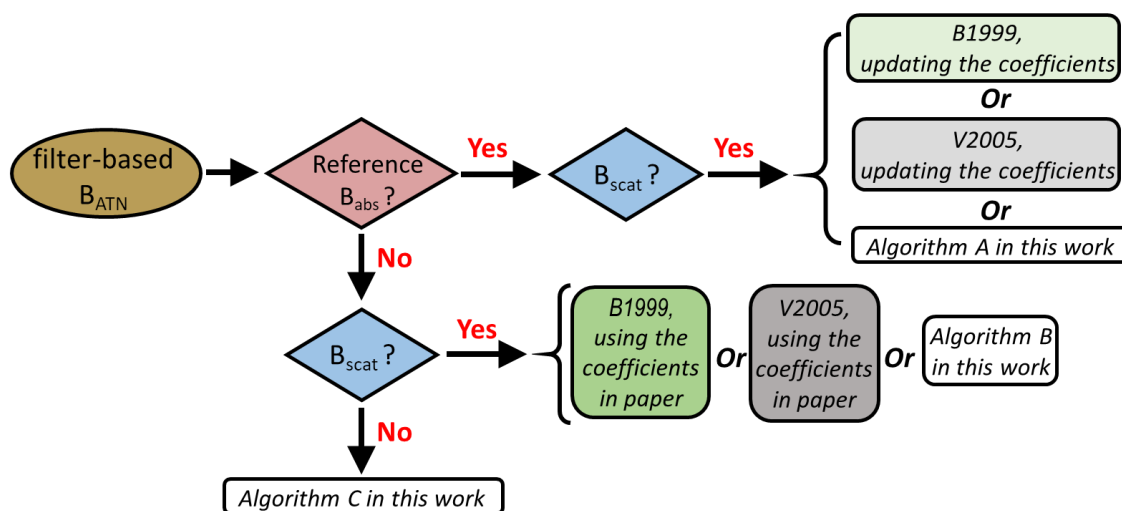
396 2.45. Application of correction algorithms

397 In developing a procedure for applying our algorithm, we envision three potential scenarios:

- 398 1. Algorithm A: The filter-based instrument is co-located with a NEPH and reference instrument
 399 providing B_{abs} . This scenario facilitates the computation of G_0 through G_7 in Eq. (9) (step 2 in
 400 the iterative process) as well as the derivation of new coefficients for existing correction
 401 algorithms. This scenario can also enable the develop of a new a set of coefficients that may
 402 be more appropriate for aerosol sources that we do not consider here.
- 403 2. Algorithm B: The filter-based instrument is co-located with a NEPH but not a reference
 404 instrument providing B_{abs} , which is perhaps the most likely scenario (at least at many long-

405 term monitoring sites). This scenario requires an initial guess of the coefficients; we provide
 406 sets of these in Table 4 below for different filter-based instruments and aerosol sources.
 407 3. Algorithm C: The filter-based instrument is deployed with neither a co-located NEPH nor a
 408 reference instrument providing B_{abs} . This scenario is the most challenging, because there are
 409 no measurements of B_{scat} to compute SSA; to address this issue, we propose the use of a non-
 410 linear relationship between SSA and AAE ($AAE = a + b \times SSA^c$) to provide an initial guess of
 411 SSA in the iterations.

412 To aid in decision-making between algorithms, we developed a flow chart for selecting appropriate
 413 correction algorithm for CLAP, TAP, and PSAP (Fig. 1). Furthermore, an Igor Pro (WaveMetrics,
 414 Inc.) based program for selecting and implementing our correction algorithms can be found in the
 415 Supplemental Material.



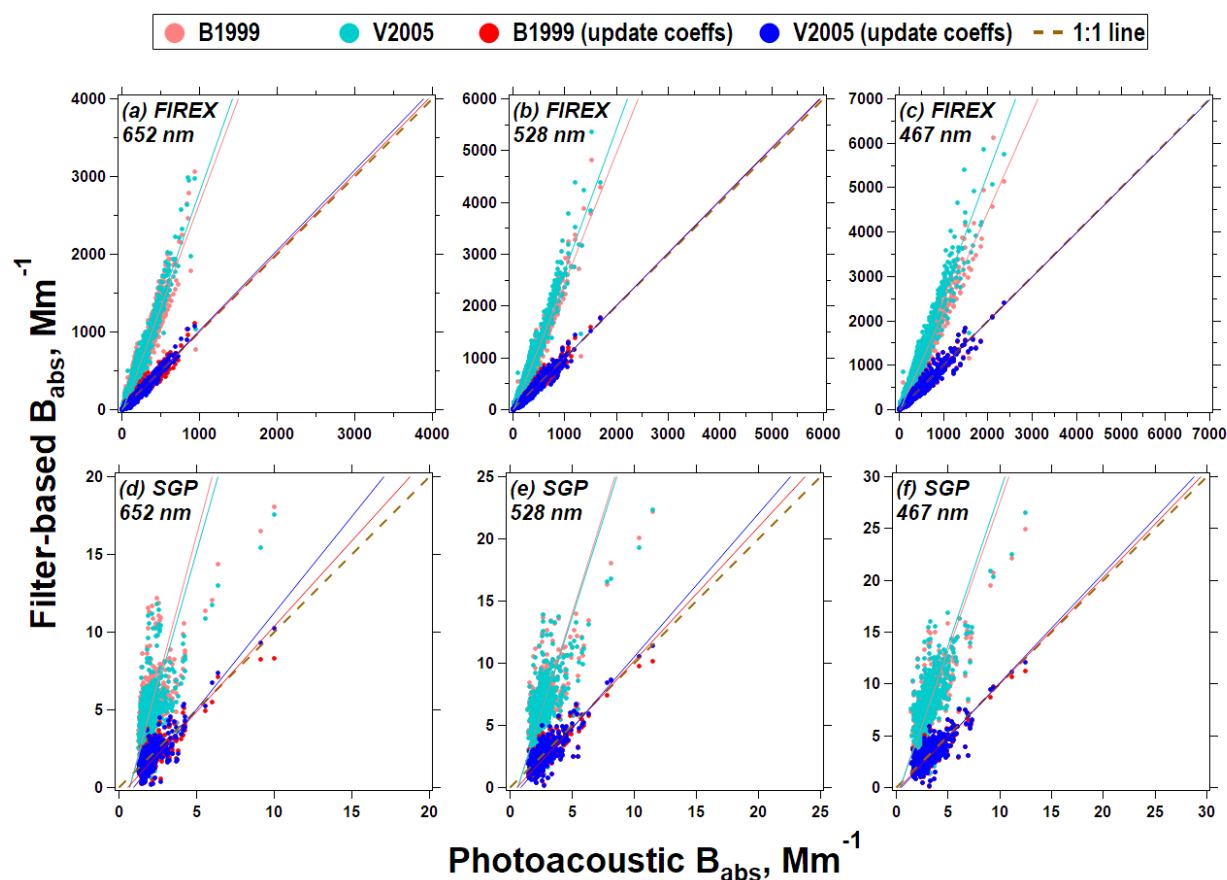
416
 417 **Figure 1.** The flow-chart for the application of correction algorithms on PSAP, CLAP, and TAP.
 418 Similar logic is followed for the AETH.

419 3. Results and discussion

420 3.1. Application of the previous algorithms on different aerosols

421 We first consider the application of the B1999 and V2005 corrections on different combinations
 422 of aerosol type and filter-based absorption photometer. Specifically, we apply the two corrections
 423 to the biomass burning data from the FIREX laboratory campaign (CLAP and TAP) as well as six
 424 months of ambient data from the SGP site (CLAP and PSAP). In doing so, we use the “default”
 425 coefficients recommended in B1999 and V2005 as well as “updated” coefficients that are
 426 estimated via regression techniques. It is important to keep in mind that the updated coefficient
 427 values of B1999 and V2005 (Table S7) are only valid for the aerosols investigated in this study.
 428 Future experiments are needed to systematically determine how the coefficients in B1999 and
 429 V2005 may change for different aerosol types. We focus on the results of the CLAP in the main
 430 text, because a CLAP is the only instrument common to deployments for both FIREX and SGP.
 431 The results of the TAP from FIREX and the PSAP from the SGP site can be found in the
 432 Supplementary Material (Table S5 and Fig. S5S11).

433 Our inter-comparison between the corrected CLAP-derived B_{abs} and reference B_{abs} for the FIREX
 434 and SGP data is provided in Fig. 2 and Table 3. For the FIREX measurements, both analyses (using
 435 the “default” coefficients and updating the coefficients) suggest good correlation (coefficient of
 436 determination (R^2) > 0.9) between the CLAP and the reference across all three wavelengths.
 437 Nevertheless, the corrections using the “default” coefficients result in over-prediction of B_{abs} by
 438 factors of ~ 2.5 . If we update the coefficients in the corrections, there is an obvious improvement
 439 in the agreement (i.e., slope ≈ 1 ; R^2 increases). The results are generally similar for SGP, although
 440 the R^2 for ambient data is generally lower for ambient data ($R^2 < 0.7$). Decreased R^2 may be due
 441 to the lower aerosol concentrations measured in ambient air, which could lead to lower signal-to-
 442 noise in the instruments. Moreover, it is worth mentioning that for both datasets (FIREX and SGP),
 443 the corrected B_{abs} from different filter-based absorption photometers using the “default”
 444 approaches does not agree with each other (slopes range from 0.69 to 1.40). However, after
 445 updating the coefficients, the slopes approach unity (Table S6).



446
 447 **Figure 2.** Inter-comparison between the CLAP-derived B_{abs} corrected by the B1999 and V2005
 448 algorithms and the reference B_{abs} at 652, 528, and 467 nm for both FIREX and SGP data. The solid
 449 lines represent linear regressions, while the dashed line is a 1:1 line.

450 **Table 3** Relationship between the CLAP-derived B_{abs} corrected by the B1999 and V2005
 451 algorithms (including updated coefficients) and the reference B_{abs} at 652, 528, and 467 nm. The
 452 relationship is achieved using major axis regression (Ayers, 2001). The value in parentheses
 453 represents the coefficient of determination (R^2) of the linear relationship.

		652 nm	528 nm	467 nm
FIREX	B1999	$y = -39 + 2.69x (0.94)$	$y = -49 + 2.50x (0.96)$	$y = -45 + 2.26x (0.97)$
	V2005	$y = -46 + 2.83x (0.96)$	$y = -57 + 2.75x (0.96)$	$y = -56 + 2.68x (0.96)$
	B1999 (update coeffs)	$y = -8.4 + 1.02x (0.96)$	$y = -7.7 + 1.01x (0.97)$	$y = -3.4 + 1.00x (0.96)$
	V2005 (update coeffs)	$y = -9.4 + 1.03x (0.97)$	$y = -7.3 + 1.01x (0.97)$	$y = -3.0 + 1.00x (0.96)$
SGP	B1999	$y = -2.60 + 3.77x (0.41)$	$y = -1.90 + 3.20x (0.49)$	$y = -0.98 + 2.85x (0.55)$
	V2005	$y = -2.50 + 3.54x (0.41)$	$y = -2.00 + 3.15x (0.48)$	$y = -1.10 + 2.96x (0.55)$
	B1999 (update coeffs)	$y = -0.29 + 1.10x (0.60)$	$y = -0.29 + 1.08x (0.63)$	$y = -0.17 + 1.03x (0.65)$
	V2005 (update coeffs)	$y = -0.57 + 1.24x (0.65)$	$y = -0.50 + 1.15x (0.67)$	$y = -0.27 + 1.06x (0.67)$

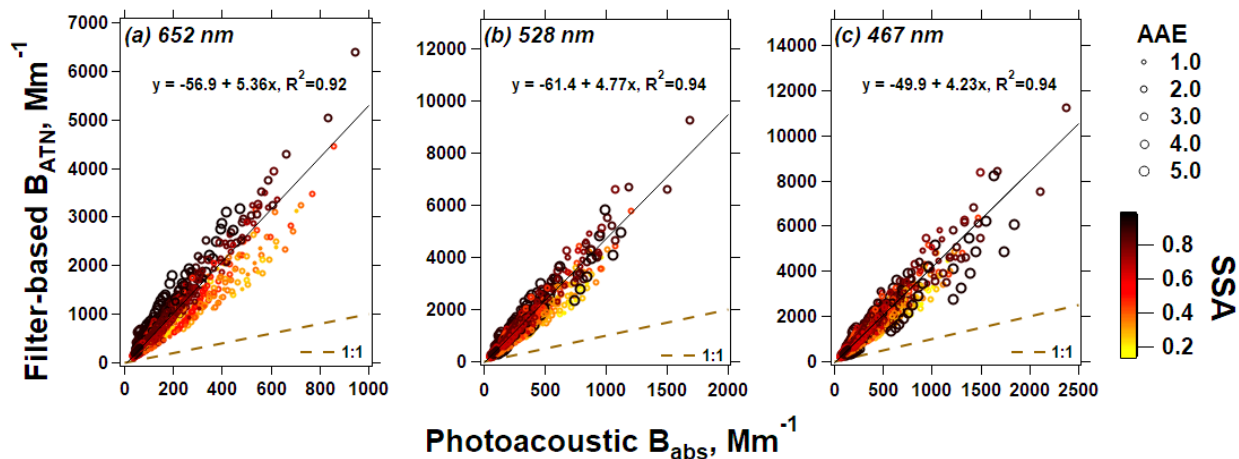
454

455 In the FIREX data, there is an apparent dependency of the updated coefficients on the wavelength
456 of light, but more importantly, on the aerosol optical properties, namely SSA and AAE (Tables
457 S7-S9). However, in the ambient data from SGP, the dependency on optical properties is less
458 obvious (Tables S10-S11). Nevertheless, all of these coefficients differ from those reported in
459 B1999 and V2005 (again, derived for the PSAP rather than the CLAP), which highlights the
460 potential need to use coefficient values that are appropriate for the instrument being used, its
461 wavelength(s) of light, and optical properties that are representative of the sampled aerosols when
462 applying correction factors to B_{ATN} .

463 3.2. Application of the new algorithms to the FIREX data

464 The co-location of the CLAP, TAP, AETH, and PAX during FIREX allows us to apply each
465 algorithm (A, B, C) to these data. Similar to Sect. 3.1, we focus our discussion on the CLAP with
466 details on the TAP and AETH presented in the Supplementary Material (Fig. ~~S5S11-S6S12~~).
467 However, we provide the recommended initial guesses in the new algorithms and the comparison
468 of absorption (corrected filter-based B_{abs} versus reference B_{abs}) for all filter-based absorption
469 photometers in Table 4 and Table 5 to help readers quickly retrieve key information of our
470 algorithms.

471 Figure 3 provides a comparison between the uncorrected B_{ATN} from the CLAP at all three
472 wavelengths, as well as photoacoustic B_{abs} interpolated to those wavelengths using AAE. For each
473 wavelength, the slopes are significantly greater than one. Moreover, there is an apparent
474 dependency on SSA and AAE in the agreement between the instruments. This is most obvious in
475 Fig. 3a (652 nm), where data with lower SSA and lower AAE (smaller markers, “brighter” colors)
476 fall below the best-fit line, while data with higher SSA and higher AAE (larger markers, “darker”
477 colors) fall above the best-fit line. This phenomenon is less clear in Fig. 3b-3c, but an apparent
478 dependency on SSA and AAE remains, which highlights the need to include both of these aerosol
479 optical properties (and appropriate interaction terms) when correcting B_{ATN} values.



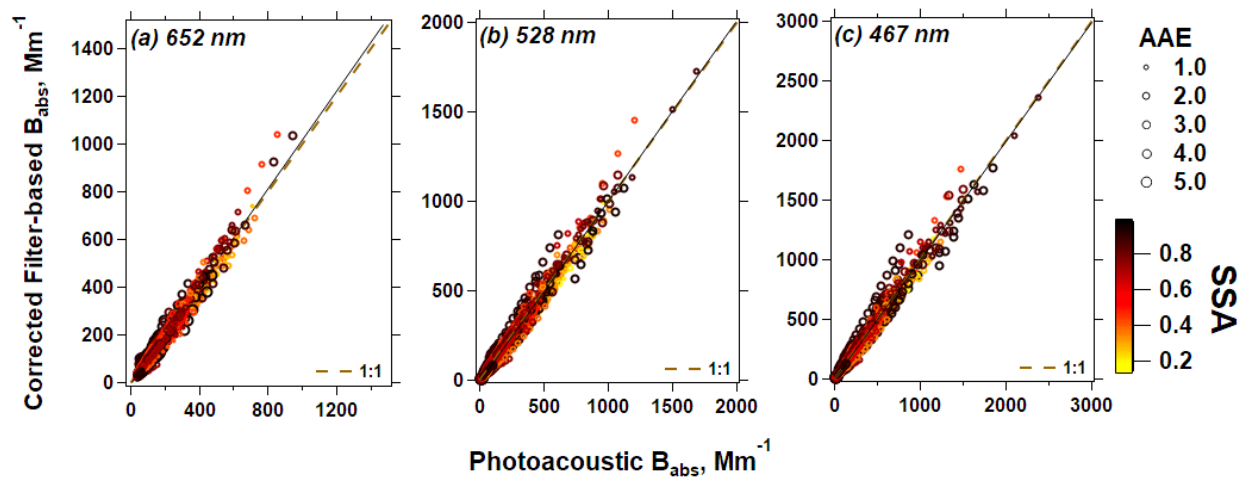
480
 481 **Figure 3.** Comparison of the uncorrected CLAP-derived B_{ATN} and the reference B_{abs} at 652, 528,
 482 and 467 nm for the FIREX data. The data points are colored by the corresponding SSA at the given
 483 wavelength. The size of data points reflects their AAE quantified by the two PAX. The solid line
 484 represents the linear regression, while the dashed line is a 1:1 line.

485 We first apply “Algorithm A” to the CLAP B_{ATN} data in Fig. 3. Using the reference B_{abs} values
 486 from the PAX (in addition to B_{scat} values), we are able to derive a set of coefficients that enable
 487 the correction of the data (Table 4). Corrected CLAP values are presented in Fig. 4 with the linear
 488 relationships presented in Table 5. The slope for each wavelength is very close to the 1:1 line,
 489 suggesting that our approach works well in correcting these data. Moreover, the heteroscedasticity
 490 that exists in Fig. 3 has been minimized after correction, and there are no apparent trends in how
 491 the data are organized in Fig. 4 due to the aerosol optical properties.

492 **Table 4** Coefficient values for Eq. (9) derived using “Algorithm A”. We recommend these as the
 493 initial guesses when implementing “Algorithm B”^a.

		G_0	G_1	G_2	G_3	G_4	G_5	G_6	G_7
CLAP (FIREX)	652 nm	0.27	-0.16	-0.18	-0.05	0.18	0.08	-0.01	0.03
	528 nm	0.30	-0.28	-0.18	-0.07	0.25	0.10	0.13	-0.17
	467 nm	0.32	-0.38	-0.20	-0.08	0.33	0.12	0.24	-0.31
TAP (FIREX)	652 nm	0.45	-0.45	0.07	-0.19	0.94	0.10	0.26	-0.35
	528 nm	0.54	-0.51	0.02	-0.26	0.76	0.20	0.38	-0.44
	467 nm	0.62	-0.59	-0.07	-0.32	0.73	0.29	0.53	-0.60
CLAP (SGP)	652 nm	0.37	-0.18	-0.34	-0.11	0.30	0.18	-0.36	0.41
	528 nm	0.40	-0.15	-0.42	-0.14	0.10	0.24	-0.17	0.25
	467 nm	0.43	-0.16	-0.45	-0.16	0.07	0.27	-0.06	0.12
PSAP (SGP)	652 nm	0.24	0.35	-0.16	-0.04	-0.47	0.07	-0.57	0.73
	528 nm	0.30	0.48	-0.26	-0.10	-0.67	0.17	-0.63	0.77
	467 nm	0.35	0.49	-0.34	-0.15	-0.69	0.23	-0.55	0.79
AETH (FIREX)	950 nm	0.47	0.17	0.01	-0.27	-0.4	0.25	-0.12	0.27
	880 nm	0.34	0.13	0.13	-0.17	0	0.10	-0.13	0.12
	660 nm	0.28	0.09	0.11	-0.12	0.15	0.05	-0.12	0.03
	590 nm	0.16	-0.08	0.26	-0.03	0.59	-0.08	-0.02	-0.19
	520 nm	0.16	-0.05	0.14	-0.01	0.54	-0.07	-0.02	-0.21
	470 nm	0.14	-0.05	0.06	0	0.53	-0.05	-0.02	-0.17
	370 nm	0.13	-0.09	0.11	0	0.59	-0.06	-0.01	0.01

494 ^aThe coefficients derived from FIREX may be more appropriate for biomass burning aerosols, and
 495 the coefficients derived from SGP may be more appropriate for rural background environments in
 496 the absence of marine aerosols and dust (see Fig. S15).
 497



498
 499 **Figure 4.** As in Fig. 3, but the CLAP-based B_{ATN} values have been corrected using our “Algorithm
 500 A”.

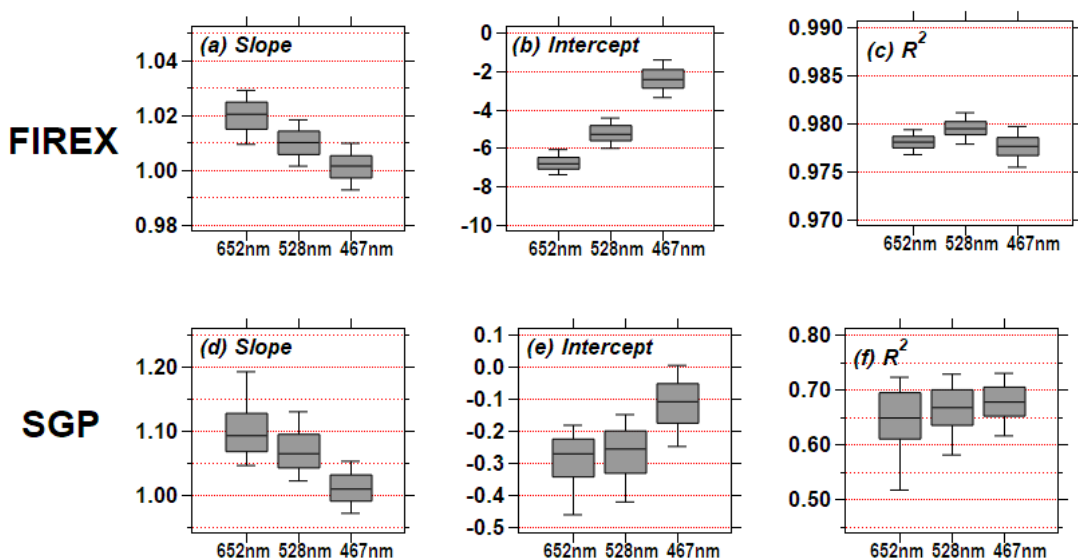
501 **Table 5** Relationship between the filter-based B_{abs} corrected by “Algorithm A” and the reference
 502 B_{abs} at the operating wavelengths for the filter-based instrument. The relationship is achieved using
 503 major axis regression (Ayers, 2001). The value in the parentheses represents the coefficient of
 504 determination (R^2) for the linear relationship.

		652 nm	528 nm	467 nm	
FIREX	CLAP	$y = -7.8 + 1.02x$ (0.98)	$y = -6.2 + 1.01x$ (0.98)	$y = -3.2 + 1.00x$ (0.98)	
	TAP	$y = -10 + 1.00x$ (0.87)	$y = -13 + 0.99x$ (0.87)	$y = -16 + 0.99x$ (0.88)	
SGP	CLAP	$y = -0.25 + 1.08x$ (0.68)	$y = -0.21 + 1.05x$ (0.67)	$y = -0.04 + 0.99x$ (0.68)	
	PSAP	$y = -0.28 + 1.10x$ (0.43)	$y = -0.24 + 1.06x$ (0.55)	$y = -0.07 + 1.00x$ (0.62)	
FIREX	AETH	950 nm	880 nm	660 nm	590 nm
		$y = -3.19 + 1.01x$ (0.82)	$y = -3.92 + 1.02x$ (0.85)	$y = -5.97 + 1.03x$ (0.88)	$y = -5.63 + 1.02x$ (0.90)
		520 nm	470 nm	370 nm	-
		$y = -2.36 + 0.99x$ (0.90)	$y = 2.93 + 0.95x$ (0.88)	$y = 18.38 + 0.89x$ (0.80)	-

505
 506 We next investigate the repeatability of the coefficient values presented in Table 4 by randomly
 507 selecting half of the measurements ($N = 1338$) from the whole FIREX dataset. By implementing
 508 “Algorithm A” to the extracted observations, we obtain new coefficient values for G_0 to G_7 . This
 509 is repeated 1000 times to obtain a distribution of coefficient values (Fig. S137). The extraction
 510 approach mimics the process of obtaining new biomass burning datasets, so that we can estimate
 511 the variability of these derived coefficients. From Fig. S7–S13 and Table S12, the derived
 512 coefficients are mostly insensitive to the different randomly-extracted datasets; most of the quartile
 513 deviation (defined as $(Q3-Q1)/2$, where $Q1$ and $Q3$ are the first and third quartile respectively) is
 514 within 0.05, except G_4 which has a quartile deviation of ~ 0.08 . Consequently, the coefficient values
 515 obtained in “Algorithm A” appear to be reasonable initial guesses to correct filter-based absorption

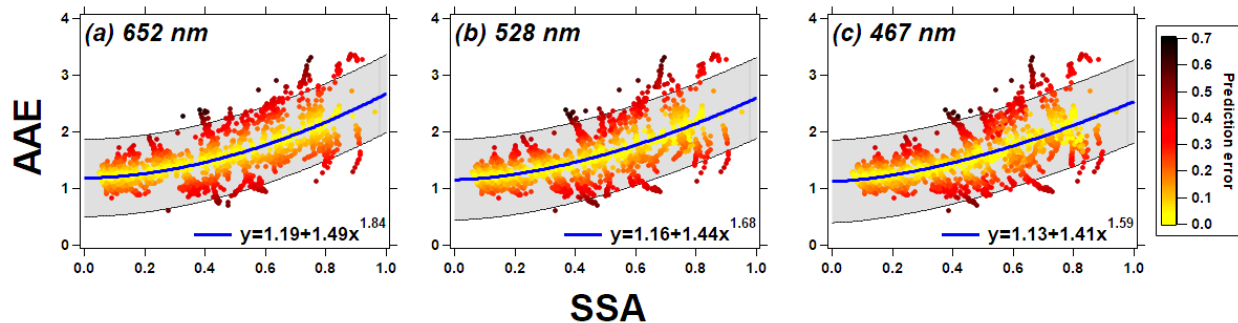
516 measurements during biomass burning events when the reference B_{abs} is unavailable, such as in
 517 “Algorithm B” and “Algorithm C”.

518 We next implement “Algorithm B” to the CLAP B_{ATN} data from Fig. 3 using the initial guesses of
 519 the coefficients derived from “Algorithm A” (Table 4) along with reference B_{scat} values. To get a
 520 sense of the variability in the results, we randomly select half of the data and applied the correction;
 521 this process is repeated 1000 times. For each iteration, we compare the corrected B_{abs} from the
 522 CLAP to the reference B_{abs} from the PAX; the resulting slope, intercept, and R^2 values are
 523 summarized as box-and-whisker plots in Fig. 5. For all three wavelengths, the slopes are close to
 524 unity, and there is good correlation between the two absorption measurements ($R^2 \approx 0.98$), which
 525 indicates that the good performance seen in Fig. 4 is independent of the reference B_{abs}
 526 measurements and our algorithm is able to correct “new” B_{ATN} . Consequently, when scattering
 527 measurements are co-located with filter-based absorption measurements, our new correction
 528 algorithm performs well.



529
 530 **Figure 5.** The box-and-whisker plots for the slope, intercept, and R^2 of the relationship between
 531 the CLAP-derived B_{abs} (corrected by “Algorithm B” in the present work) and PAX-derived B_{abs} for
 532 all three wavelengths. For details on how these values were generated, please refer to the text.

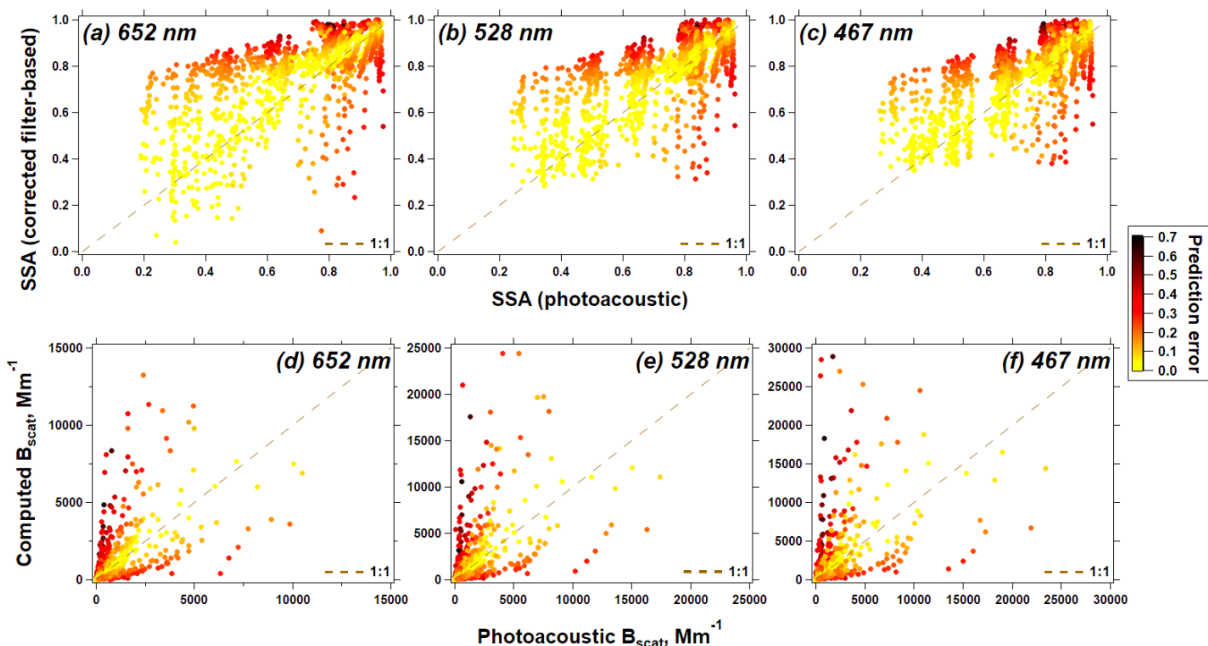
533 Lastly, we apply “Algorithm C” to the data in Fig. 3. However, we first require a functional
 534 relationship between AAE and SSA, because in this scenario, the CLAP B_{ATN} values are the only
 535 data input to the algorithm (and therefore, SSA is unknown). Liu et al. (2014) proposed that a
 536 power function can describe this relationship ($\text{AAE} = a + b \times \text{SSA}^c$); we present these data from
 537 FIREX along with power function fits (and associated prediction intervals) in Fig. 6. To define
 538 AAE in this figure, we fit a power-law relationship to the three B_{ATN} values from the CLAP;
 539 similarly, we define SSA using interpolated B_{scat} from the PAX and B_{ATN} from the CLAP (The
 540 rationale for using B_{ATN} is that if “Algorithm C” were to be implemented in practice, only B_{ATN}
 541 would be available). In Fig. 6, the data points are colored by “prediction error”, effectively a metric
 542 to quantify how well the power function reproduces the individual data points. Although there is
 543 a fair amount of error in some of these points, we still obtain an SSA-AAE relationship required
 544 to initialize “Algorithm C”.



545

546 **Figure 6.** AAE plotted against SSA for the FIREX data. In the figures, AAE was computed using a
 547 power-law fit across all three wavelengths, and SSA was computed using the interpolated B_{scat}
 548 from the two PAX and the reported B_{ATN} from the CLAP. The data points are colored by their
 549 prediction error ($(\text{“true” AAE} - \text{“calculated” AAE}) / \text{“calculated” AAE}$).

550 Even though there is uncertainty in the SSA vs. AAE relationship used in “Algorithm C”, after
 551 corrections have been applied, the filter-based B_{abs} for the CLAP agrees well with the independent
 552 reference B_{abs} ; the slopes for all wavelengths are slightly greater than 1 (1.03-1.05) and the R^2
 553 values are all high (0.97-0.98). However, even though the absorption measurements are corrected
 554 well, there still remains large uncertainties in values of inferred scattering. Examples of this are
 555 provided in Fig. 7, where we compare the SSA inferred from the PAX to the SSA inferred from
 556 “Algorithm C” as well as B_{scat} for each wavelength. Generally speaking, data that are better
 557 represented by the SSA vs. AAE relationship (i.e., smaller prediction error) results in better
 558 agreement with the reference for both SSA and B_{scat} , but there is also a clear divergence from the
 559 1:1 line in Fig. 7a-c as SSA decreases. Therefore, even though “Algorithm C” performs well at
 560 correcting filter-based B_{ATN} to agree with the reference B_{abs} , estimates of final SSA values should
 561 be considered to be uncertain.



562
 563 **Figure 7.** Comparison of SSA (a-c) and B_{scat} (d-f) at the three wavelengths for the FIREX data.
 564 Vertical axis: values output from “Algorithm C”; horizontal axis: values calculated using the
 565 photoacoustic B_{abs} and B_{scat} .

566 To explore the universal behavior of the new algorithms across different instruments, in addition
 567 to the CLAP, we next apply the new our algorithms to the other filter-based absorption photometers
 568 operated during the FIREX study (TAP and AETH). Consistent with what we observed for the
 569 CLAP results, the corrected TAP- and AETH-derived B_{abs} is in good agreement with the
 570 photoacoustic B_{abs} (as demonstrated in Table 4 and Table 5, as well as Fig. [S5S11-S6S12](#)).
 571 Moreover, the corrected B_{abs} from the three filter-based instruments agrees with each other for all
 572 three wavelengths (Table 6), confirming the universal nature of our algorithm.

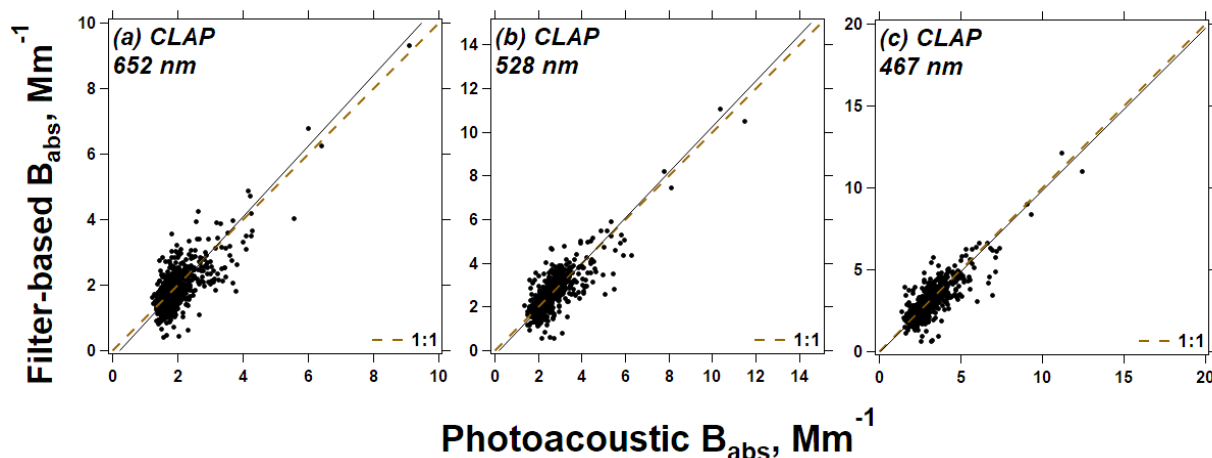
573 **Table 6** Inter-comparison between different filter-based B_{abs} corrected by “Algorithm A” in the
 574 present work. The value in the parentheses represents the coefficient of determination (R^2) of the
 575 linear relationship.

	FIREX: CLAP vs. TAP	FIREX: CLAP vs. AETH	FIREX: TAP vs. AETH	SGP: CLAP vs. PSAP
652 nm	$y = 1.84 + 1.02x$ (0.89)	$y = 4.17 + 0.94x$ (0.87)	$y = -0.31 + 0.99x$ (0.82)	$y = -0.04 + 0.99x$ (0.70)
528 nm	$y = 5.75 + 1.02x$ (0.88)	$y = 3.70 + 0.91x$ (0.85)	$y = -6.38 + 0.98x$ (0.82)	$y = -0.11 + 1.02x$ (0.73)
467 nm	$y = 10.57 + 1.01x$ (0.88)	$y = 0.45 + 0.98x$ (0.83)	$y = -13.62 + 1.04x$ (0.79)	$y = -0.11 + 1.02x$ (0.76)

576
 577 **3.3. Application of the new algorithms to ambient data**

578 To test our algorithms further, we extended our work to ambient data collected the DOE SGP site
 579 during the time period which the PASS-3 was operational. From the SGP data, we derived a
 580 different set of coefficients for ambient data using “Algorithm A”, which differ from those derived
 581 for FIREX (Table 4). The results presented in Fig. 8 and Table 5 suggest that our new algorithm
 582 works at least as well as B1999 and V2005 on this dataset (both with updated coefficients). The

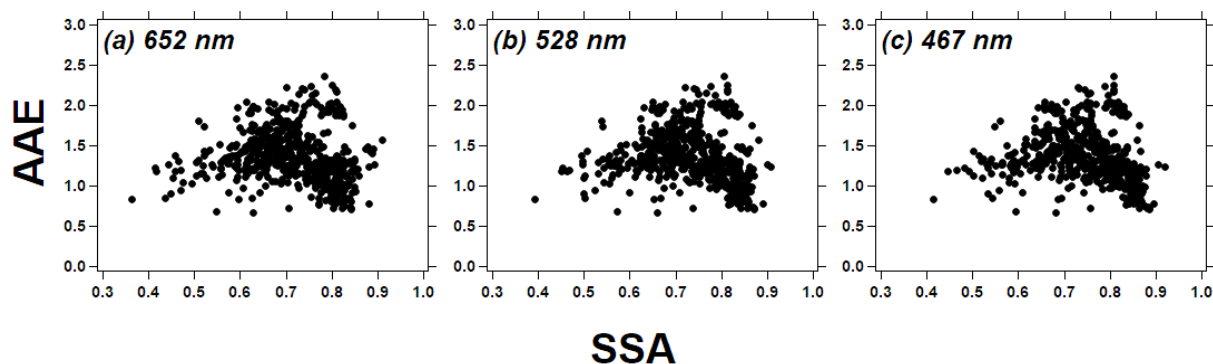
583 repeatability of the coefficient values in “Algorithm A” is confirmed for the SGP measurements
584 using the same procedure as described in Sect. 3.2 (see results in Fig. S7-S13 and Table S12).



585
586 **Figure 8.** Inter-comparison between the CLAP-derived B_{abs} corrected by “Algorithm A” in the
587 present work and reference B_{abs} at 652, 528, and 467 nm for the ambient data at the SGP study
588 area. The solid line represents the linear regression, while the dashed line is a 1:1 line.

589 On the SGP data, we see similar performance to the FIREX data when we apply “Algorithm B”,
590 where we again sampled half of the CLAP data, used the initial guesses derived in “Algorithm A”,
591 and repeated this process 1000 times. Although the slopes tend to be larger than 1 (i.e., the
592 corrected CLAP B_{abs} remains high relative to the PASS B_{abs}), the results still represent an
593 improvement over B1999 and V2005 using their recommended coefficients for their correction
594 equations.

595 Implementing “Algorithm C” is challenging for ambient data, because there is no distinct power
596 function relationship in AAE vs. SSA (Fig. 9); this is consistent with other field studies reporting
597 both SSA and AAE (e.g., Backman et al. (2014) and Lim et al. (2018)). Our approach described
598 here is only appropriate for ambient aerosols that follow a power function, such as sites impacted
599 by biomass burning. Nevertheless, we did apply this to a subset of the SGP data where the AAE-
600 SSA prediction error is within 30% ($N = 86$), and for this subset of data, “Algorithm C” works
601 fairly well (slopes ≈ 0.95 ; see Fig. S148). Therefore, while “Algorithm C” may have utility for
602 ambient data, we advise caution when using this algorithm since the aerosols influencing the site
603 may not be represented by a clear AAE-SSA power function (e.g., when biomass burning and
604 coarse aerosols are equally prevalent at a long-term monitoring site).



605
 606 **Figure 9.** AAE plotted against SSA for the SGP ambient data. The power law fit ($AAE = a + b \times SSA^c$)
 607 is performed on SSA ($SSA = B_{scat}/(B_{scat} + B_{ATN})$) and AAE computed by three-wavelength B_{ATN} .

608 These new algorithms are also applicable to the PSAP deployed at the SGP site. The results of the
 609 correction for the PSAP are presented in Table 5 and Fig. S5S11, and the recommended initial
 610 guesses when implementing “Algorithm B” to PSAP- B_{ATN} at ambient environments are given in
 611 Table 4. As expected, there is good agreement between corrected PSAP- and CLAP- B_{abs} (Table
 612 6).

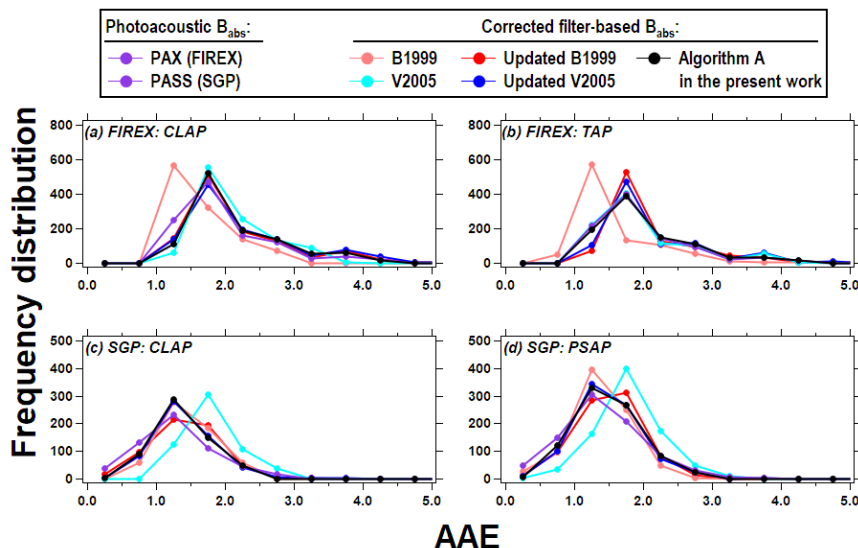
613 To investigate if our algorithms are suitable to correct B_{abs} obtained from different ambient
 614 environments, the aerosol properties from the SGP site are compared to those from the other
 615 NOAA/ESRL observational sites. We use the similar “AAE-SAE space” as that in Cappa et al.
 616 (2016) and Schmeisser et al. (2017) to infer dominant aerosol types (e.g., BC, BrC, dust, mixed
 617 dust/BC/BrC, see Fig. S15). Our results of AAE and SAE overlap with most of the values from
 618 the NOAA/ESRL sites, except when marine aerosols or dust contribute to the local aerosol
 619 emissions. Though none of the NOAA/ESRL sites fall into the clusters of BC or BC/BrC, some of
 620 our data can represent the optical properties of aerosols from these clusters. Therefore, we highlight
 621 that our algorithm developed by the SGP data may have the potential to be generalized to a variety
 622 of environmental conditions, but we would need to validate this using observations from more
 623 studies.

624 3.4. Impact of the implemented correction algorithm on aerosol optical properties

625 In addition to the direct comparisons of B_{abs} between the filter-based and photoacoustic
 626 measurements, we compare derived optical properties (AAE and SSA) from different instruments
 627 to assess the algorithms’ performance on derived aerosol optical properties. For example, we have
 628 discussed the discrepancy of SSA between the filter-based and photoacoustic measurements when
 629 implementing “Algorithm C” in Sect. 3.2. In this section we will more broadly discuss the impact
 630 of different correction algorithms on AAE and SSA.

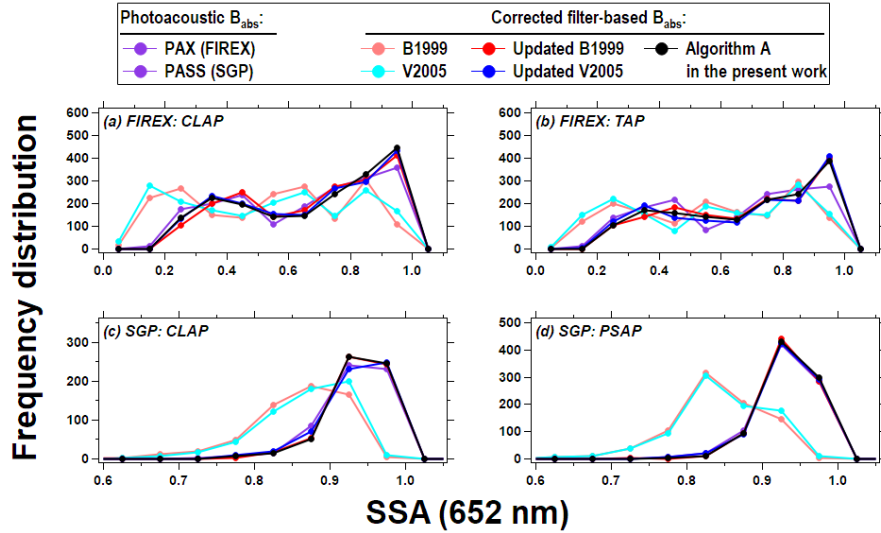
631 In Fig. 10, we present the frequency distribution of AAE for both FIREX and SGP data generated
 632 from different campaign/instrument pairs using different correction approaches. For the FIREX
 633 data (Fig. 10a-b), most corrections (with the exception of the “default” B1999) are consistent with
 634 the photoacoustic data, while for the SGP data (Fig. 10c-d), most corrections (with the exception
 635 of “default” V2005) are consistent with the photoacoustic data. However, updating the coefficients
 636 for B1999 and V2005 improves the agreement with the photoacoustic data. The 50% difference
 637 that exists between the B1999 and V2005 algorithms in all panels in Fig. 10 are consistent with

638 previous studies. For example, both Backman et al. (2014) and Davies et al. (2019) found that the
 639 V2005-derived AAE is greater than B1999-derived AAE by 33% to 50% for ambient aerosols.
 640 Therefore, we highlight that the default coefficients in B1999 and V2005 may have some
 641 limitations when deriving AAE using the corrected B_{abs} ; instead, updating the coefficients or using
 642 the new algorithm proposed in this work may yield more robust AAE results.



643
 644 **Figure 10.** The frequency distribution of AAE calculated for different instrument/correction
 645 combinations of multi-wavelength B_{abs} .

646 Similar to Fig. 10, we also investigate the distribution of SSA computed by using corrected B_{abs}
 647 along with B_{scat} . We provide the results at 652 nm as an example in the main text (Fig. 11); figures
 648 for 528 nm and 467 nm can be found in the Supplementary Material (Fig. [S9-S16](#) and [S10-S17](#)).
 649 For both FIREX and SGP data, the SSA obtained using the new algorithm agree very well with
 650 the B1999 and V2005 but only when their coefficients have been updated. Calculations of SSA
 651 using B1999 and V2005 with their recommended coefficients suggest that these values may be
 652 biased low, which follows the over-estimation of corrected B_{abs} demonstrated in Fig. 2.

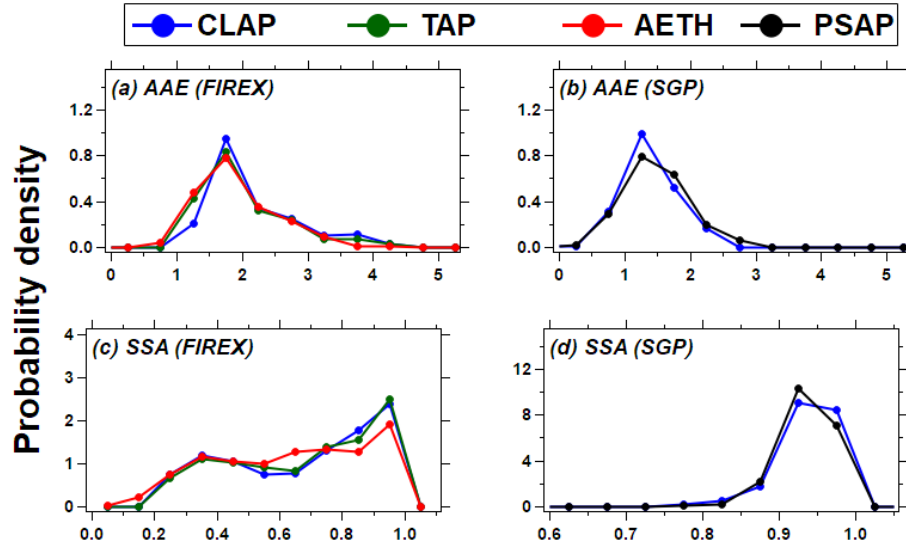


653

654 **Figure 11.** The frequency distribution of SSA (652 nm) calculated for different
 655 instrument/correction combinations of B_{abs} and B_{scat} .

656 Moreover, we plot similar figures as Fig. 10-11 using all algorithms (A, B, and C). As shown in
 657 Fig. S4S18, the results using “Algorithm B” agrees very well with those using “Algorithm A”,
 658 but the use of “Algorithm C” results in some obvious discrepancies compared to the photoacoustic
 659 reference, again highlighting the potential for large uncertainty using this algorithm.

660 In Fig. 12, we directly compare the distributions of both AAE and SSA at 652 nm for all of the
 661 filter-based absorption photometers considered here, using our “Algorithm A” to correct the B_{ATN}
 662 data. For both datasets, after the corrections have been applied, there are only marginal differences
 663 of the AAE (Fig. 10a and 10b) derived by different instruments. Similarly, there is good agreement
 664 among the SSA values when using corrected- B_{abs} from different instruments (Fig. 10c and 10d).
 665 Overall, the derived properties using the new correction are consistent across all instruments,
 666 suggesting its universality.



667

668 **Figure 12** The probability density of AAE and SSA (652 nm) derived by different filter-based
 669 photometers B_{abs} (corrected by “Algorithm A” in the present work). Note that the number of total
 670 observations vary across instruments.

671 3.5. Uncertainty of the new algorithms

672 In this section, we estimate the uncertainty of the new algorithms due to both measurement
 673 uncertainties of the instruments and the uncertainties of parameter computation. We then simulate
 674 the propagated uncertainty in the corrected filter-based B_{abs} reported in this paper.

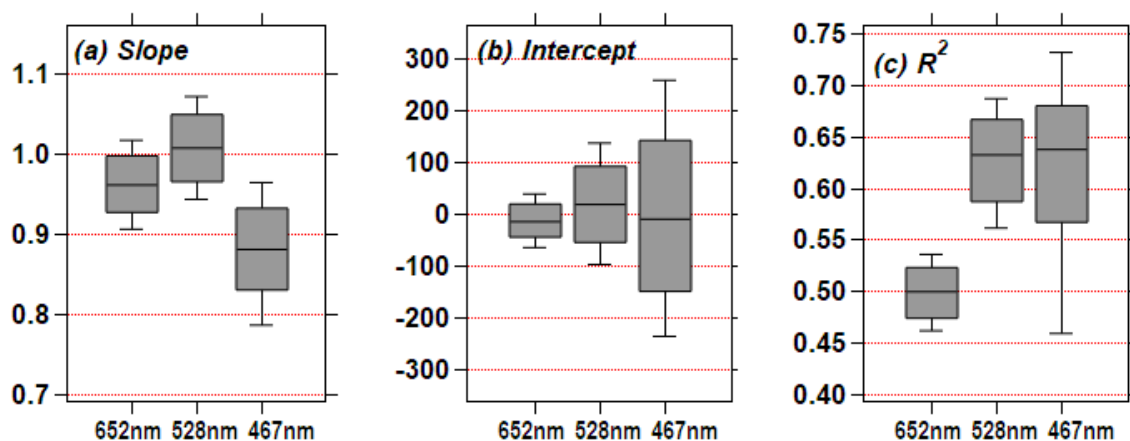
675 Measurement uncertainties of the instruments considered here have been reported in previous work
 676 (e.g., (Anderson et al., 1996; Nakayama et al., 2015; Ogren et al., 2017; Sherman et al., 2015)) and
 677 are summarized in Table 1. The typical sources of measurement uncertainty of the aerosol
 678 instruments include: 1) instrument noise (often associated with the averaging time); 2) calibration
 679 uncertainties (such as the accuracy of the operating wavelengths and the properties of the
 680 calibration materials); 3) standard temperature and pressure (STP) correction uncertainties
 681 (Sherman et al., 2015); and 4) flow rate uncertainties. Additional uncertainties that are specific to
 682 filter-based absorption photometers include spot size and filter medium corrections (Bond et al.,
 683 1999; Ogren et al., 2017). Regardless, these values all tend to be $\leq 30\%$, which is consistent with
 684 other commonly-used aerosol instrumentation.

685 Because correction algorithms for filter-based absorption instruments also require aerosol optical
 686 properties, the algorithms’ performance will be affected by these values as well. For example,
 687 uncertainties in SSA are directly related to uncertainties associated with B_{abs} and B_{scat} , which are
 688 both included in our simulations. However, capturing uncertainties in AAE is more complex, as
 689 AAE can be computed by either “ 2λ fit” (a linear fit using B_{abs} at two wavelengths) or “ 3λ fit”
 690 (same as the power fit used in the present work). Davies et al. (2019) used the 3λ fit to calculate
 691 AAE and compared this to calculations using 662 nm and 785 nm (i.e., $\text{AAE}_{662/785}$), finding that
 692 the 3λ results was about 50% greater. Moreover, similar differences (-35% to 85%) can exist
 693 comparing two different 2λ combinations ($\text{AAE}_{440/870}$ and $\text{AAE}_{675/870}$), depending on the
 694 contribution of brown carbon to absorption at 440 nm (Wang et al., 2016). However, based on Fig.
 695 [S12-S19](#) and [S13-S20](#), we demonstrate small ($< \sim 10\%$) differences in the calculated values of AAE

696 using our Algorithm A using different 2λ combinations for linear fits and the 3λ power-law fit,
 697 when considering both FIREX and SGP data. Consequently, we do not include AAE calculation
 698 uncertainty in our simulation.

699 In our simulations, the propagated uncertainty of corrected B_{abs} is estimated by implementing the
 700 new algorithm to datasets in which filter-based B_{ATN} , reference B_{abs} , and B_{scat} are subject to
 701 measurement uncertainties. The full procedure is outlined in the Supplementary Material, but we
 702 provide a brief overview of our Monte Carlo approach here. First, we create a synthetic dataset (n
 703 = 500 records) that defines B_{abs} at 652 nm and AAE that is intended to represent biomass burning.
 704 Values of B_{ATN} and SSA are then computed using the relationships presented in Fig. 3 and Fig. 6,
 705 respectively. Respective uncertainties associated with each of these values are applied following
 706 Table 1, assuming that these follow a normal distribution. We then applied “Algorithm B” to the
 707 B_{ATN} dataset, repeated 1000 times, to quantify overall uncertainty associated with our correction
 708 algorithm.

709 Figure 13 provides a graphical summary of our uncertainty simulation results, which was derived
 710 by fitting linear equations to the “true” B_{abs} value (that we defined) and the “corrected” B_{abs} values
 711 (outputs of each iteration). Considering the slopes (Fig. 12a), our algorithm can generally
 712 reproduce the “true” value within 10% at 652 nm and 528 nm, but the performance is slightly
 713 degraded at 467 nm. The median intercept for our simulations is close to zero, but the interquartile
 714 range increases with decreasing wavelength (Fig. 12b), suggesting that the uncertainty may
 715 increase at shorter wavelengths. The coefficients of determination (Fig. 12c) range from 0.47 (652
 716 nm) to 0.68 (467 nm), showing that the algorithm may be less precise if large measurement
 717 uncertainties exist. Even though these sources of uncertainty exist when implementing our
 718 correction algorithms and propagate through to the corrected values, we argue that our new
 719 algorithm will “standardize” uncertainties across corrected B_{abs} values from filter-based absorption
 720 photometers. Moreover, the new algorithms perform, at least, better than the previous algorithms
 721 with “default” coefficients, or as well as the previous algorithms with updated coefficients.



722
 723 **Figure 13.** The box-and-whisker plots (slope, intercept, and R^2) for the Monte Carlo simulation of
 724 the relationship between the CLAP-derived B_{abs} (corrected by “Algorithm B” in the present work)
 725 and “true” B_{abs} for all three wavelengths.

726 4. Conclusions

727 Filter-based absorption instruments are widely used at global observational sites due to their
728 relatively low cost, fast response, and easy operation. Despite the existence of different correction
729 algorithms to correct the filter-based B_{abs} measurements, these are not “standardized” as
730 differences in corrected B_{abs} values exist across different instrument/correction combinations, even
731 when the instruments are co-located. This study provides a systematic evaluation of the previous
732 correction algorithms (B1999 and V2005 corrections) on the CLAP and similar instruments (TAP
733 and PSAP) using both laboratory-generated biomass burning emissions and ambient aerosols. We
734 also developed “universal” correction algorithms that are applicable to any filter-based absorption
735 photometer (e.g., PSAP, CLAP, TAP, AETH), which will have utility for any historic or future
736 filter-based absorption measurements and which have the potential to standardize absorption
737 coefficients across all filter-based instruments. This latter point is demonstrated in Table 6 and Fig.
738 12 in that there is good agreement across all filter-based absorption photometers when applying
739 our corrections to both biomass burning and ambient data. In practice, we anticipate that our
740 Algorithm B will be most common, because at long-term monitoring sites, filter-based absorption
741 photometers are typically co-located with a nephelometer.

742 Using the existing corrections on our CLAP measurements, we find that the corrected B_{abs}
743 overestimate photoacoustic B_{abs} by factors of ~ 2.6 (biomass burning aerosols) and ~ 3.2 (ambient
744 aerosols). Similar overestimations of absorption by filter-based instruments are seen in the results
745 of TAP from the FIREX study and PSAP deployed at the SGP. Comparing between B1999 and
746 V2005, B_{abs} corrected by the two corrections differ by -6% to 18% . These discrepancies in our
747 results are consistent with those reported for the inter-comparisons between filter-based and
748 photoacoustic absorption instruments (e.g., (Arnott et al., 2003; Davies et al., 2019; Li et al., 2019;
749 Müller et al., 2011a)).

750 Overall, our new developed algorithms (A, B, and C) perform well on correcting B_{abs} for different
751 filter-based absorption photometers (CLAP, TAP, PSAP, and AETH) from both biomass burning
752 and ambient measurements. Our work suggests that if the filter-based instrument is co-operated
753 with a reference absorption instrument and a NEPH at field for a period, researchers can compute
754 site-specific initial guesses (same as “Algorithm A” in the present work). Otherwise, either
755 “Algorithm B” or “Algorithm C” proposed in this paper can be used to correct the filter-based
756 measurements. In “Algorithm B” when a filter-based absorption photometer is co-located with a
757 NEPH but without a reference instrument, the set of coefficients yield in this work (Table 4) can
758 be used as initial guesses to implement the algorithm. In “Algorithm C” when a filter-based
759 absorption photometer is operated by itself, a “representative” relationship between AAE and SSA
760 can be used to estimate SSA from AAE at each step in the iterative process, but we advise caution
761 if this relationship is not monotonic (e.g., as in the ambient data from SGP and from Backman et
762 al. (2014) and Lim et al. (2018)). The only scenario not included in the present work is that the
763 filter-based absorption photometer is co-located with a reference absorption instrument, but no
764 instrument for scattering. However, under this scenario, one could simply use the photoacoustic
765 B_{abs} data because no filter-induced biases exist for those instruments.

766 In terms of the aerosol optical properties (AAE and SSA) computed by different corrections, the
767 new algorithm suggests no bias of AAE and SSA when compared to that derived by updated-
768 B1999 and updated-V2005 for both aerosol datasets.

769 However, the new algorithm is not without limitations. First, we used the photoacoustic B_{abs} as the
770 reference to develop the algorithm and the initial guess of the coefficients; meanwhile, some
771 studies argue that photoacoustic absorption is not a “ground truth” (e.g., (Lack et al., 2006; Lewis
772 et al., 2008)). Thus, we simulate the propagated uncertainty of our algorithms considering the
773 measurement uncertainties due to the photoacoustic B_{abs} (as well as B_{ATN} and B_{scat}) and find that
774 the corrected B_{abs} can be biased by -17% to 5%, depending on the operated wavelength. Although
775 potential bias due to the precision of photoacoustic B_{abs} cannot be excluded, using the universal
776 algorithm to correct the filter-based B_{abs} will at least eliminate correction-related biases among
777 different filter-based instruments. Second, we only tested the algorithms with data from biomass
778 burning and ambient measurements. It is unclear how the algorithms will work for other absorbing
779 aerosols (e.g., dominated by fossil fuel emissions or mineral dust). Further evaluation of the
780 performance of the new algorithm on other aerosol sources may help to address this issue.
781 Regardless, we argue that our approach can standardize reported absorption coefficients at long-
782 term monitoring sites, which has the potential to yield a better data set with which to evaluate
783 chemistry-climate models.

784 **Code and data availability.** The code for the algorithm has been developed in Igor Pro
785 (WaveMetrics Inc.). The package is available and fully described in the Supplementary Material.
786 The FIREX aerosol products are available at <https://esrl.noaa.gov/csd/project/firex>. The SGP
787 aerosol products are available at <https://www.archive.arm.gov/discovery/> (February 2013–July
788 2013, 36° 36' 18.0" N, 97° 29' 6.0" W: Southern Great Plains Central Facility, data set accessed
789 01/16/19).

790 **Competing interests.** The authors declare that they have no conflict of interest.

791 **Acknowledgements.** The project was funded by NOAA Climate Program Office Grant
792 NA16OAR4310109. The ambient data at SGP site in Lamont (OK, USA) were obtained from the
793 atmospheric radiation measurement (ARM) user facility, a U.S. Department of Energy (DOE)
794 Office of Science user facility managed by the Office of Biological and Environmental Research.
795 The authors would like to specifically thank Allison Aiken (Los Alamos National Laboratory) for
796 useful discussions. The authors greatly acknowledge Vanessa Selimovic, and Robert Yokelson
797 from University of Montana for lending us the PAX-405, Patrick Sheridan, John Ogren, and Derek
798 Hageman from NOAA for lending us the CLAP, and Anthony Prenni from the National Park
799 Service for lending us the AETH during the FIREX campaign. Nick Good (Colorado State
800 University), Jim Roberts (NOAA) and Carsten Warneke (NOAA) are acknowledged for their on-
801 site support at FSL.

802

803 5. References

- 804 Allan, D. W.: Statistics of atomic frequency standards, *Proc. IEEE*, 54(2), 221–230,
805 doi:10.1109/PROC.1966.4634, 1966.
- 806 Alvarado, M. J., Lonsdale, C. R., Macintyre, H. L., Bian, H., Chin, M., Ridley, D. A., Heald, C.
807 L., Thornhill, K. L., Anderson, B. E., Cubison, M. J., Jimenez, J. L., Kondo, Y., Sahu, L. K., Dibb,
808 J. E. and Wang, C.: Evaluating model parameterizations of submicron aerosol scattering and
809 absorption with in situ data from ARCTAS 2008, *Atmos. Chem. Phys.*, 16(14), 9435–9455,
810 doi:10.5194/acp-16-9435-2016, 2016.
- 811 Anderson, T. L., Covert, D. S., Marshall, S. F., Laucks, M. L., Charlson, R. J., Waggoner, A. P.,
812 Ogren, J. A., Caldow, R., Holm, R. L., Quant, F. R., Sem, G. J., Wiedensohler, A., Ahlquist, N. A.
813 and Bates, T. S.: Performance Characteristics of a High-Sensitivity, Three-Wavelength, Total
814 Scatter/Backscatter Nephelometer, *J. Atmos. Ocean. Technol.*, 13(5), 967–986, doi:10.1175/1520-
815 0426, 1996.
- 816 Andrews, E., Sheridan, P. J. and Ogren, J. A.: Seasonal differences in the vertical profiles of
817 aerosol optical properties over rural Oklahoma, *Atmos. Chem. Phys.*, 11(20), 10661–10676,
818 doi:10.5194/acp-11-10661-2011, 2011.
- 819 Andrews, E., Sheridan, P. J., Ogren, J. A., Hageman, D., Jefferson, A., Wendell, J., Alástuey, A.,
820 Alados-Arboledas, L., Bergin, M., Ealo, M., Hallar, A. G., Hoffer, A., Kalapov, I., Keywood, M.,
821 Kim, J., Kim, S.-W., Kolonjari, F., Labuschagne, C., Lin, N.-H., Macdonald, A., Mayol-Bracero,
822 O. L., McCubbin, I. B., Pandolfi, M., Reisen, F., Sharma, S., Sherman, J. P., Sorribas, M. and Sun,
823 J.: Overview of the NOAA/ESRL Federated Aerosol Network, *Bull. Am. Meteorol. Soc.*, 100(1),
824 123–135, doi:10.1175/BAMS-D-17-0175.1, 2019.
- 825 Arnott, W. P., Moosmüller, H., Sheridan, P. J., Ogren, J. A., Raspert, R., Slaton, W. V., Hand, J.
826 L., Kreidenweis, S. M. and Collett, J. L.: Photoacoustic and filter-based ambient aerosol light
827 absorption measurements: Instrument comparisons and the role of relative humidity, *J. Geophys.*
828 *Res.*, 108(D1), 4034, doi:10.1029/2002JD002165, 2003.
- 829 Arnott, W. P., Hamasha, K., Moosmüller, H., Sheridan, P. J. and Ogren, J. A.: Towards Aerosol
830 Light-Absorption Measurements with a 7-Wavelength Aethalometer: Evaluation with a
831 Photoacoustic Instrument and 3-Wavelength Nephelometer, *Aerosol Sci. Technol.*, 39(1), 17–29,
832 doi:10.1080/027868290901972, 2005.
- 833 Ayers, G. P.: Comment on regression analysis of air quality data, *Atmos. Environ.*, 35(13), 2423–
834 2425, doi:10.1016/S1352-2310(00)00527-6, 2001.
- 835 Backman, J., Virkkula, A., Vakkari, V., Beukes, J. P., Van Zyl, P. G., Josipovic, M., Piketh, S.,
836 Tiitta, P., Chiloane, K., Petäjä, T., Kulmala, M. and Laakso, L.: Differences in aerosol absorption
837 Ångström exponents between correction algorithms for a particle soot absorption photometer
838 measured on the South African Highveld, *Atmos. Meas. Tech.*, 7(12), 4285–4298,
839 doi:10.5194/amt-7-4285-2014, 2014.
- 840 Bergstrom, R. W., Pilewskie, P., Russell, P. B., Redemann, J., Bond, T. C., Quinn, P. K. and Sierau,
841 B.: Spectral absorption properties of atmospheric aerosols, *Atmos. Chem. Phys.*, 7(23), 5937–5943,
842 doi:10.5194/acp-7-5937-2007, 2007.

- 843 Bond, T. C. and Bergstrom, R. W.: Light absorption by carbonaceous particles: An investigative
844 review, *Aerosol Sci. Technol.*, 40(1), 27–67, doi:10.1080/02786820500421521, 2006.
- 845 Bond, T. C., Anderson, T. L. and Campbell, D.: Calibration and Intercomparison of Filter-Based
846 Measurements of Visible Light Absorption by Aerosols, *Aerosol Sci. Technol.*, 30(6), 582–600,
847 doi:10.1080/027868299304435, 1999.
- 848 Boucher, O.: *Atmospheric Aerosols*, Springer Netherlands, Dordrecht., 2015.
- 849 Cappa, C. D., Lack, D. A., Burkholder, J. B. and Ravishankara, A. R.: Bias in Filter-Based Aerosol
850 Light Absorption Measurements Due to Organic Aerosol Loading: Evidence from Laboratory
851 Measurements, *Aerosol Sci. Technol.*, 42(12), 1022–1032, doi:10.1080/02786820802389285,
852 2008.
- 853 Cappa, C. D., Kolesar, K. R., Zhang, X., Atkinson, D. B., Pekour, M. S., Zaveri, R. A., Zelenyuk,
854 A. and Zhang, Q.: Understanding the optical properties of ambient sub- and supermicron
855 particulate matter: results from the CARES 2010 field study in northern California, *Atmos. Chem.*
856 *Phys.*, 16(10), 6511–6535, doi:10.5194/acp-16-6511-2016, 2016.
- 857 Chen, S., Russell, L. M., Cappa, C. D., Zhang, X., Kleeman, M. J., Kumar, A., Liu, D. and
858 Ramanathan, V.: Comparing black and brown carbon absorption from AERONET and surface
859 measurements at wintertime Fresno, *Atmos. Environ.*, 199, 164–176,
860 doi:10.1016/j.atmosenv.2018.11.032, 2019.
- 861 Collaud Coen, M., Weingartner, E., Apituley, A., Ceburnis, D., Fierz-Schmidhauser, R., Flentje,
862 H., Henzing, J. S., Jennings, S. G., Moerman, M., Petzold, A., Schmid, O. and Baltensperger, U.:
863 Minimizing light absorption measurement artifacts of the Aethalometer: evaluation of five
864 correction algorithms, *Atmos. Meas. Tech.*, 3(2), 457–474, doi:10.5194/amt-3-457-2010, 2010.
- 865 Davies, N. W., Fox, C., Szpek, K., Cotterell, M. I., Taylor, J. W., Allan, J. D., Williams, P. I.,
866 Trembath, J., Haywood, J. M. and Langridge, J. M.: Evaluating biases in filter-based aerosol
867 absorption measurements using photoacoustic spectroscopy, *Atmos. Meas. Tech.*, 12(6), 3417–
868 3434, doi:10.5194/amt-12-3417-2019, 2019.
- 869 Drinovec, L., Gregorič, A., Zotter, P., Wolf, R., Bruns, E. A., Prévôt, A. S. H., Petit, J.-E., Favez,
870 O., Sciare, J., Arnold, I. J., Chakrabarty, R. K., Moosmüller, H., Filep, A. and Močnik, G.: The
871 filter-loading effect by ambient aerosols in filter absorption photometers depends on the coating
872 of the sampled particles, *Atmos. Meas. Tech.*, 10(3), 1043–1059, doi:10.5194/amt-10-1043-2017,
873 2017.
- 874 Fischer, D. Al and Smith, G. D.: A portable, four-wavelength, single-cell photoacoustic
875 spectrometer for ambient aerosol absorption, *Aerosol Sci. Technol.*, 52(4), 393–406,
876 doi:10.1080/02786826.2017.1413231, 2018.
- 877 Horvath, H.: Atmospheric light absorption—A review, *Atmos. Environ. Part A. Gen. Top.*, 27(3),
878 293–317, doi:10.1016/0960-1686(93)90104-7, 1993.
- 879 Jiang, Y., Yang, J., Gagné, S., Chan, T. W., Thomson, K., Fofie, E., Cary, R. A., Rutherford, D.,
880 Comer, B., Swanson, J., Lin, Y., Van Rooy, P., Asa-Awuku, A., Jung, H., Barsanti, K., Karavalakis,
881 G., Cocker, D., Durbin, T. D., Miller, J. W. and Johnson, K. C.: Sources of variance in BC mass
882 measurements from a small marine engine: Influence of the instruments, fuels and loads, *Atmos.*

883 Environ., 182, 128–137, doi:10.1016/j.atmosenv.2018.03.008, 2018.

884 Kirchstetter, T. W. and Novakov, T.: Controlled generation of black carbon particles from a
885 diffusion flame and applications in evaluating black carbon measurement methods, *Atmos.*
886 *Environ.*, 41(9), 1874–1888, doi:10.1016/j.atmosenv.2006.10.067, 2007.

887 Koss, A. R., Sekimoto, K., Gilman, J. B., Selimovic, V., Coggon, M. M., Zarzana, K. J., Yuan, B.,
888 Lerner, B. M., Brown, S. S., Jimenez, J. L., Krechmer, J., Roberts, J. M., Warneke, C., Yokelson,
889 R. J. and de Gouw, J.: Non-methane organic gas emissions from biomass burning: identification,
890 quantification, and emission factors from PTR-ToF during the FIREX 2016 laboratory experiment,
891 *Atmos. Chem. Phys.*, 18(5), 3299–3319, doi:10.5194/acp-18-3299-2018, 2018.

892 Lack, D. A., Lovejoy, E. R., Baynard, T., Pettersson, A. and Ravishankara, A. R.: Aerosol
893 Absorption Measurement using Photoacoustic Spectroscopy: Sensitivity, Calibration, and
894 Uncertainty Developments, *Aerosol Sci. Technol.*, 40(9), 697–708,
895 doi:10.1080/02786820600803917, 2006.

896 Lack, D. A., Cappa, C. D., Covert, D. S., Baynard, T., Massoli, P., Sierau, B., Bates, T. S., Quinn,
897 P. K., Lovejoy, E. R. and Ravishankara, A. R.: Bias in Filter-Based Aerosol Light Absorption
898 Measurements Due to Organic Aerosol Loading: Evidence from Ambient Measurements, *Aerosol*
899 *Sci. Technol.*, 42(12), 1033–1041, doi:10.1080/02786820802389277, 2008a.

900 Lack, D. A., Lerner, B., Granier, C., Baynard, T., Lovejoy, E., Massoli, P., Ravishankara, A. R.
901 and Williams, E.: Light absorbing carbon emissions from commercial shipping, *Geophys. Res.*
902 *Let.*, 35(13), L13815, doi:10.1029/2008GL033906, 2008b.

903 Lack, D. A., Moosmüller, H., McMeeking, G. R., Chakrabarty, R. K. and Baumgardner, D.:
904 Characterizing elemental, equivalent black, and refractory black carbon aerosol particles: A review
905 of techniques, their limitations and uncertainties, *Anal. Bioanal. Chem.*, 406(1), 99–122,
906 doi:10.1007/s00216-013-7402-3, 2014.

907 Laing, J. R., Jaffe, D. A. and Hee, J. R.: Physical and optical properties of aged biomass burning
908 aerosol from wildfires in Siberia and the Western USA at the Mt. Bachelor Observatory, *Atmos.*
909 *Chem. Phys.*, 16(23), 15185–15197, doi:10.5194/acp-16-15185-2016, 2016.

910 Levenberg, K.: A method for the solution of certain non-linear problems in least squares, *Q. Appl.*
911 *Math.*, 2(2), 164–168, 1944.

912 Lewis, K., Arnott, W. P., Moosmüller, H. and Wold, C. E.: Strong spectral variation of biomass
913 smoke light absorption and single scattering albedo observed with a novel dual-wavelength
914 photoacoustic instrument, *J. Geophys. Res. Atmos.*, 113(16), 1–14, doi:10.1029/2007JD009699,
915 2008.

916 Li, H., Lamb, K. D., Schwarz, J. P., Selimovic, V., Yokelson, R. J., McMeeking, G. R. and May,
917 A. A.: Inter-comparison of black carbon measurement methods for simulated open biomass
918 burning emissions, *Atmos. Environ.*, 206, 156–169, doi:10.1016/j.atmosenv.2019.03.010, 2019.

919 Lim, S., Lee, M., Kim, S.-W. and Laj, P.: Sulfate alters aerosol absorption properties in East Asian
920 outflow, *Sci. Rep.*, 8(1), 5172, doi:10.1038/s41598-018-23021-1, 2018.

921 Liu, S., Aiken, A. C., Arata, C., Dubey, M. K., Stockwell, C. E., Yokelson, R. J., Stone, E. A.,
922 Jayarathne, T., Robinson, A. L., DeMott, P. J. and Kreidenweis, S. M.: Aerosol single scattering

923 albedo dependence on biomass combustion efficiency: Laboratory and field studies, *Geophys. Res.*
924 *Letts.*, 41(2), 742–748, doi:10.1002/2013GL058392, 2014.

925 McMeeking, G. R., Fortner, E., Onasch, T. B., Taylor, J. W., Flynn, M., Coe, H. and Kreidenweis,
926 S. M.: Impacts of nonrefractory material on light absorption by aerosols emitted from biomass
927 burning, *J. Geophys. Res. Atmos.*, 119(21), 12,272–12,286, doi:10.1002/2014JD021750, 2014.

928 Moosmüller, H., Chakrabarty, R. K. and Arnott, W. P.: Aerosol light absorption and its
929 measurement: A review, *J. Quant. Spectrosc. Radiat. Transf.*, 110(11), 844–878,
930 doi:10.1016/j.jqsrt.2009.02.035, 2009.

931 Moteki, N., Kondo, Y. and Nakamura, S.: Method to measure refractive indices of small
932 nonspherical particles: Application to black carbon particles, *J. Aerosol Sci.*, 41(5), 513–521,
933 doi:10.1016/j.jaerosci.2010.02.013, 2010.

934 Müller, T., Henzing, J. S., de Leeuw, G., Wiedensohler, A., Alastuey, A., Angelov, H., Bizjak, M.,
935 Collaud Coen, M., Engström, J. E., Gruening, C., Hillamo, R., Hoffer, A., Imre, K., Ivanow, P.,
936 Jennings, G., Sun, J. Y., Kalivitis, N., Karlsson, H., Komppula, M., Laj, P., Li, S.-M., Lunder, C.,
937 Marinoni, A., Martins dos Santos, S., Moerman, M., Nowak, A., Ogren, J. A., Petzold, A., Pichon,
938 J. M., Rodriguez, S., Sharma, S., Sheridan, P. J., Teinilä, K., Tuch, T., Viana, M., Virkkula, A.,
939 Weingartner, E., Wilhelm, R. and Wang, Y. Q.: Characterization and intercomparison of aerosol
940 absorption photometers: result of two intercomparison workshops, *Atmos. Meas. Tech.*, 4(2), 245–
941 268, doi:10.5194/amt-4-245-2011, 2011a.

942 Müller, T., Laborde, M., Kassell, G. and Wiedensohler, A.: Design and performance of a three-
943 wavelength LED-based total scatter and backscatter integrating nephelometer, *Atmos. Meas. Tech.*,
944 4(6), 1291–1303, doi:10.5194/amt-4-1291-2011, 2011b.

945 Müller, T., Virkkula, A. and Ogren, J. A.: Constrained two-stream algorithm for calculating
946 aerosol light absorption coefficient from the Particle Soot Absorption Photometer, *Atmos. Meas.*
947 *Tech.*, 7(12), 4049–4070, doi:10.5194/amt-7-4049-2014, 2014.

948 Nakayama, T., Kondo, Y., Moteki, N., Sahu, L. K., Kinase, T., Kita, K. and Matsumi, Y.: Size-
949 dependent correction factors for absorption measurements using filter-based photometers: PSAP
950 and COSMOS, *J. Aerosol Sci.*, 41(4), 333–343, doi:10.1016/j.jaerosci.2010.01.004, 2010.

951 Nakayama, T., Suzuki, H., Kagamitani, S., Ikeda, Y., Uchiyama, A. and Matsumi, Y.:
952 Characterization of a Three Wavelength Photoacoustic Soot Spectrometer (PASS-3) and a
953 Photoacoustic Extinctionmeter (PAX), *J. Meteorol. Soc. Japan. Ser. II*, 93(2), 285–308,
954 doi:10.2151/jmsj.2015-016, 2015.

955 Ogren, J. A.: Comment on “ Calibration and Intercomparison of Filter-Based Measurements of
956 Visible Light Absorption by Aerosols ,” *Aerosol Sci. Technol.*, 44(December), 589–591,
957 doi:10.1080/02786826.2010.482111, 2010.

958 Ogren, J. A., Wendell, J., Andrews, E. and Sheridan, P. J.: Continuous light absorption photometer
959 for long-term studies, *Atmos. Meas. Tech.*, 10(12), 4805–4818, doi:10.5194/amt-10-4805-2017,
960 2017.

961 Olson, M. R., Victoria Garcia, M., Robinson, M. A., Van Rooy, P., Dietenberger, M. A., Bergin,
962 M. and Schauer, J. J.: Investigation of black and brown carbon multiple-wavelength-dependent

963 light absorption from biomass and fossil fuel combustion source emissions, *J. Geophys. Res.*
964 *Atmos.*, 120(13), 6682–6697, doi:10.1002/2014JD022970, 2015.

965 Rajesh, T. A. and Ramachandran, S.: Black carbon aerosol mass concentration, absorption and
966 single scattering albedo from single and dual spot aethalometers: Radiative implications, *J.*
967 *Aerosol Sci.*, 119(January), 77–90, doi:10.1016/j.jaerosci.2018.02.001, 2018.

968 Saturno, J., Pöhlker, C., Massabò, D., Brito, J., Carbone, S., Cheng, Y., Chi, X., Ditas, F., Hrab
969 De Angelis, I., Morán-Zuloaga, D., Pöhlker, M. L., Rizzo, L. V., Walter, D., Wang, Q., Artaxo, P.,
970 Prati, P. and Andreae, M. O.: Comparison of different Aethalometer correction schemes and a
971 reference multi-wavelength absorption technique for ambient aerosol data, *Atmos. Meas. Tech.*,
972 10(8), 2837–2850, doi:10.5194/amt-10-2837-2017, 2017.

973 Schmeisser, L., Andrews, E., Ogren, J. A., Sheridan, P., Jefferson, A., Sharma, S., Kim, J. E.,
974 Sherman, J. P., Sorribas, M., Kalapov, I., Arsov, T., Angelov, C., Mayol-Bracero, O. L.,
975 Labuschagne, C., Kim, S.-W., Hoffer, A., Lin, N.-H., Chia, H.-P., Bergin, M., Sun, J., Liu, P. and
976 Wu, H.: Classifying aerosol type using in situ surface spectral aerosol optical properties, *Atmos.*
977 *Chem. Phys.*, 17(19), 12097–12120, doi:10.5194/acp-17-12097-2017, 2017.

978 Schmid, O., Artaxo, P., Arnott, W. P., Chand, D., Gatti, L. V., Frank, G. P., Hoffer, A., Schnaiter,
979 M. and Andreae, M. O.: Spectral light absorption by ambient aerosols influenced by biomass
980 burning in the Amazon Basin. I: Comparison and field calibration of absorption measurement
981 techniques, *Atmos. Chem. Phys.*, 6(11), 3443–3462, doi:10.5194/acp-6-3443-2006, 2006.

982 Schwarz, J. P., Spackman, J. R., Fahey, D. W., Gao, R. S., Lohmann, U., Stier, P., Watts, L. A.,
983 Thomson, D. S., Lack, D. A., Pfister, L., Mahoney, M. J., Baumgardner, D., Wilson, J. C. and
984 Reeves, J. M.: Coatings and their enhancement of black carbon light absorption in the tropical
985 atmosphere, *J. Geophys. Res.*, 113(D3), D03203, doi:10.1029/2007JD009042, 2008.

986 Sedlacek, A. J.: DOE/SC-ARM-TR-156 Aethalometer™ Instrument Handbook, DOE Office of
987 Science Atmospheric Radiation Measurement (ARM) Program., 2016.

988 Selimovic, V., Yokelson, R. J., Warneke, C., Roberts, J. M., de Gouw, J., Reardon, J. and Griffith,
989 D. W. T.: Aerosol optical properties and trace gas emissions by PAX and OP-FTIR for laboratory-
990 simulated western US wildfires during FIREX, *Atmos. Chem. Phys.*, 18(4), 2929–2948,
991 doi:10.5194/acp-18-2929-2018, 2018.

992 Sheridan, P. J., Arnott, W. P., Ogren, J. A., Andrews, E., Atkinson, D. B., Covert, D. S.,
993 Moosmüller, H., Petzold, A., Schmid, B., Strawa, A. W., Varma, R. and Virkkula, A.: The Reno
994 Aerosol Optics Study: An Evaluation of Aerosol Absorption Measurement Methods, *Aerosol Sci.*
995 *Technol.*, 39(1), 1–16, doi:10.1080/027868290901891, 2005.

996 Sherman, J. P., Sheridan, P. J., Ogren, J. A., Andrews, E., Hageman, D., Schmeisser, L., Jefferson,
997 A. and Sharma, S.: A multi-year study of lower tropospheric aerosol variability and systematic
998 relationships from four North American regions, *Atmos. Chem. Phys.*, 15(21), 12487–12517,
999 doi:10.5194/acp-15-12487-2015, 2015.

1000 Springston, S. R.: DOE/SC-ARM-TR-176 Radiance Research Particle Soot/Absorption
1001 Photometer Instrument Handbook, DOE Office of Science Atmospheric Radiation Measurement
1002 (ARM) Program (United States)., 2016.

- 1003 Subramanian, R., Roden, C. A., Boparai, P. and Bond, T. C.: Yellow Beads and Missing Particles:
1004 Trouble Ahead for Filter-Based Absorption Measurements, *Aerosol Sci. Technol.*, 41(6), 630–637,
1005 doi:10.1080/02786820701344589, 2007.
- 1006 Vignati, E., Karl, M., Krol, M., Wilson, J., Stier, P. and Cavalli, F.: Sources of uncertainties in
1007 modelling black carbon at the global scale, *Atmos. Chem. Phys.*, 10(6), 2595–2611,
1008 doi:10.5194/acp-10-2595-2010, 2010.
- 1009 Virkkula, A.: Correction of the Calibration of the 3-wavelength Particle Soot Absorption
1010 Photometer (3λ PSAP), *Aerosol Sci. Technol.*, 44(8), 706–712,
1011 doi:10.1080/02786826.2010.482110, 2010.
- 1012 Virkkula, A., Ahlquist, N. C., Covert, D. S., Arnott, W. P., Sheridan, P. J., Quinn, P. K. and
1013 Coffman, D. J.: Modification, calibration and a field test of an instrument for measuring light
1014 absorption by particles, *Aerosol Sci. Technol.*, 39(1), 68–83, doi:10.1080/027868290901963,
1015 2005.
- 1016 Virkkula, A., Mäkelä, T., Hillamo, R., Yli-Tuomi, T., Hirsikko, A., Hämeri, K. and Koponen, I.
1017 K.: A simple procedure for correcting loading effects of aethalometer data, *J. Air Waste Manag.*
1018 *Assoc.*, 57(10), 1214–1222, doi:10.3155/1047-3289.57.10.1214, 2007.
- 1019 Virkkula, A., Chi, X., Ding, A., Shen, Y., Nie, W., Qi, X., Zheng, L., Huang, X., Xie, Y., Wang,
1020 J., Petäjä, T. and Kulmala, M.: On the interpretation of the loading correction of the aethalometer,
1021 *Atmos. Meas. Tech.*, 8(10), 4415–4427, doi:10.5194/amt-8-4415-2015, 2015.
- 1022 Wang, X., Heald, C. L., Sedlacek, A. J., de Sá, S. S., Martin, S. T., Alexander, M. L., Watson, T.
1023 B., Aiken, A. C., Springston, S. R. and Artaxo, P.: Deriving brown carbon from multiwavelength
1024 absorption measurements: method and application to AERONET and Aethalometer observations,
1025 *Atmos. Chem. Phys.*, 16(19), 12733–12752, doi:10.5194/acp-16-12733-2016, 2016.
- 1026 Weingartner, E., Saathoff, H., Schnaiter, M., Streit, N., Bitnar, B. and Baltensperger, U.:
1027 Absorption of light by soot particles: Determination of the absorption coefficient by means of
1028 aethalometers, *J. Aerosol Sci.*, 34(10), 1445–1463, doi:10.1016/S0021-8502(03)00359-8, 2003.